# COLOR IMAGE ENHANCEMENT TECHNIQUES FOR ENDOSCOPIC IMAGES

A Thesis Submitted to the

College of Graduate Studies and Research

in Partial Fulfillment of the Requirements

for the degree of Master of Science

in the Department of Electrical and Computer Engineering

University of Saskatchewan

Saskatoon, Saskatchewan, Canada

By

Mohammad Shamim Imtiaz

# PERMISSION TO USE

In presenting this thesis in partial fulfilment of the requirements for a Master of Science degree from the University of Saskatchewan, I agree that the Libraries of this University may make it freely available for inspection. I further agree that permission for copying of this thesis in any manner, in whole or in part, for scholarly purposes may be granted by the professor or professors who supervised my thesis work or, in their absence, by the Head of the Department or the Dean of the College in which my thesis work was done. It is understood that any copying or publication or use of this thesis or parts thereof for financial gain shall not be allowed without my written permission. It is also understood that due recognition shall be given to me and to the University of Saskatchewan in any scholarly use which may be made of any material in my thesis.

Requests for permission to copy or to make other use of material in this thesis in whole or part should be addressed to:

Head of the Department of Electrical and Computer Engineering

University of Saskatchewan,

57 Campus Drive, Saskatoon,

Saskatchewan, S7N 5A9,

Canada.

# ABSTRACT

Modern endoscopes play an important role in diagnosing various gastrointestinal (GI) tract related diseases. Although clinical findings of modern endoscopic imaging techniques are encouraging, there still remains much room for improvement of image quality. Of greatest concern, endoscopic images suffer from various degradations, such as specular highlights, non-uniform brightness and poor contrast. As a result, gastroenterologists often face difficulty in successfully identifying the subtle features, such as mucosal surface and structures, pit patterns, size and pattern of micro-vessels, tissue and vascular characteristics, superficial layer of mucosal and abnormal growths in endoscopic images. The improved visual quality of images can provide better diagnosis.

This paper presents two proposed post-processing techniques for enhancing the subtle features of endoscopic images. The first proposed technique is named as endoscopic image enhancement based on adaptive sigmoid function and space-variant color reproduction (ASSVCR). It is achieved in two stages: image enhancement at gray level followed by color reproduction with the help of space variant chrominance mapping. Image enhancement is achieved by performing adaptive sigmoid function and uniform distribution of sigmoid pixels. Then color reproduction is used to generate new chrominance components. The second proposed technique is named as tri-scan. It is achieved in three stages: (1) Tissue and surface enhancement: a modified linear unsharp masking is used to sharpen the surface and edges of tissue and vascular characteristics, (2) Mucosa layer enhancement: an adaptive sigmoid function similar to the ASSVCR technique is employed on the R plane of the image to highlight the superficial layers of mucosa, (3) Color tone enhancement: the pixels are uniformly distributed to

create a different color effect to highlight mucosa structures, superficial layers of mucosa and tissue characteristics.

Both techniques are compared with other related works. Several performance metrics like focus value, statistic of visual representation, measurement of uniform distribution, color similarity test, color enhancement factor (CEF) and time complexity are used to assess the performance. The results showed improved performance compared to similar existing methods. In the post-processed images, we have observed that the ASSVCR can enhance and highlight pit patterns, tissue and vascular characteristics, mucosa structures and abnormal growths. It cannot highlight size and pattern of micro-vessels, and superficial layer of mucosa. In contrast, tri-scan can enhance and highlight all above mentioned features of endoscopic images.

# ACKNOWLEDGEMENTS

I would like to start by praising the almighty God, Allah, the creator of the heavens and the earth. I owe a debt of gratitude to my supervisor Dr. Khan Wahid, without whom this research would not have been possible. I am most grateful for his guidance and valuable advice. I also thank him for providing a supportive environment for the research.

This research was supported by Grand Challenges Canada (GCC) stars in Global Health and Natural Science and Engineering Research Council of Canada (NSERC). I would also like to acknowledge the Department of Electrical and Computer Engineering of University of Saskatchewan for awarding me the Devolved scholarship, Canada Foundation for Innovation (CFI) and Canadian Microelectronics Corporation (CMC) for providing the lab infrastructure and development tools.

Finally, I am grateful to my parents, brother, colleagues and especially to my fiancé for their support and inspiration.

# TABLE OF CONTENTS

# LIST OF FIGURES

# LIST OF TABLES

# LIST OF ABBREVIATIONS

| | |
|---|---|
| AFI | Auto Florescence Imaging |
| AHE | Adaptive Histogram Equalization |
| BPDFHE | Brightness Preserving Dynamic Fuzzy Histogram Equalization |
| BPDHE | Brightness Preserving Dynamic Histogram Equalization |
| CLAHE | Contrast Limited Adaptive Histogram Equalization |
| CT | Computerized tomography |
| CTE | Color Tone Enhancement |
| CAD | Computer Aided Detection |
| CCD | Charge Coupled Device |
| CMOS | Complementary Metal Oxide Semiconductor |
| CT | Computerized tomography |
| CE | Chromoendoscopy |
| CM | Colorfulness Matric |
| CDF | Cumulative Distribution Function |
| CEF | Color Enhancement Factor |
| CPU | Central processing unit |
| DCT | Discrete Cosine Transform |
| FICE | Fuji Intelligent Color Enhancement |
| GI | Gastrointestinal |
| HBF | high boost filtering |
| HSV | Hue Saturation Value |
| ME | Magnified Endoscopy |
| MSSIM | Mean Structure Similarity Index |
| MLE | Mucosal Layer Enhancement |
| NBI | Narrow Band Imaging |
| PC | Personal Computer |
| RGB | Red Green Blue |
| RAM | Random-access memory |
| SHSIM | Structure and Hue Similarity |
| SSIM | Structural Similarity |
| TSE | Tissue and Surface Enhancement |
| WCE | Wireless Capsule Endoscopy |
| WLI | White Light Imaging |

# Chapter 1: Introduction

## 1.1 Overview of endoscopic systems

Gastrointestinal (GI) tract related diseases, such as ulcerative colitis, digestive gland disorders, tumors, defected polyps, stomach and colon cancers, are now great threats to human health [1]. According to statistics of Hong Kong Cancer Registry [2], the number of bowel cancer cases in Hong Kong ranked the second highest of all cancer cases. The diseases in the GI tract have higher chance of being cured if they are detected early.

The best way to detect and diagnose GI diseases is viewing the GI tract directly, which is possible using endoscopy. The traditional or flexible wired endoscopy system is a device consisting of a flexible tube and illumination system that offers diagnosis of upper and lower GI tract but the small intestine cannot be reached. Moreover, it can increase the risk of intestine perforation and the chances of cross-contamination [3]. Other technologies, such as colonoscopy and enteroscopy, can be used to diagnose the GI tract, but they have drawbacks such as, pancreatitis, hemorrhage, intestine perforation and invasiveness [4] [5]. Wireless capsule endoscopy (WCE) [6] [7], introduced by Given Imaging in 2000, offers a non-invasive way to diagnose small intestine. In WCE, there is a pill shaped device that consists of a short focal length CMOS camera, light source, battery and transmitter. After swallowing, it is propelled by muscle contractions and begins to capture the images when moving forward along GI tract. Meanwhile, the images are transmitted wirelessly to a data recorder mounted around patient's waist. The entire process lasts about eight to ten hours. Finally, the images are downloaded into a computer and gastroenterologists can view the images and diagnose for potential diseases. Additionally, this procedure offers an opportunity for off-line post-processing and computer-aided diagnosis [8].

## 1.2 Overview of endoscopic imaging

Although clinical findings of WCE are encouraging, there is still room for improvement [9]. One limitation with the present WCE is poor image quality. The following reasons play important roles in the degradation of image quality. First, the hardware limitations of WCE restrict the usage of high definition camera sensors, thereby producing low resolution images. On the contrary, traditional wired endoscopy has superior performance on this aspect since no power limitation exists [10]. In WCE, CMOS image sensor is used as it offers the advantages of low power consumption, but the image quality is lower than that produced by CCD image sensor [11]. Moreover, inadequate imaging conditions such as low illumination and complex circumstances in the GI tract further degrade the quality of the image [7]. Furthermore, the short focal length image camera can only view limited distances creating effects of depth that are not ideal. Not only the hardware limitations and low power consumption of WCE; the very nature of GI tract also plays a role in the degradations. The GI organ has its own convolution, bending and waving natures; therefore, inhomogeneous brightness and poor contrast inevitably occurs in the images [6] [7] [12] [13]. Additionally, the images captured by traditional wired endoscopy often cannot detect all the features of GI tract such as defected polyps, mucosa or lesions structures, tissue and vascular characteristics and pit patterns [14] [15] [16] [17].

There are both in-chip and post-processing systems that can enhance certain mucosal or vascular characteristics of endoscopic images. Two examples of in-chip technologies are narrow band imaging (NBI) [18] and auto-florescence imaging (AFI) [14]. These techniques often use special rotating filters in front of the light source to sequentially generate red, blue and green light for tissue illumination. Although the image acquisition process in the two cases are similar, they differ in the light sources and wavelengths of the filters used. Despite of their improved

image quality, these techniques increase hardware complexity and power consumption of the endoscopic system. Virtual chromoendoscopy (CE) is a post-processing system that decomposes images into various wavelengths and produces reconstructed image with enhanced mucosal surface [15]. The combination of wavelengths varies depending on the location of GI tract, which increase the complexity of CE. Fig.1.1 presents some examples of white light imaging (WLI), NBI, AFI and CE. Here, WLI refers to the imaging technology that is used by both wired endoscopy and WCE normally. We can see that some features are better visible in NBI, AFI and CE images compared to WLI images.

There are other techniques that have been used to enhance medical endoscopic images. These techniques will be briefly discussed in the next chapter.

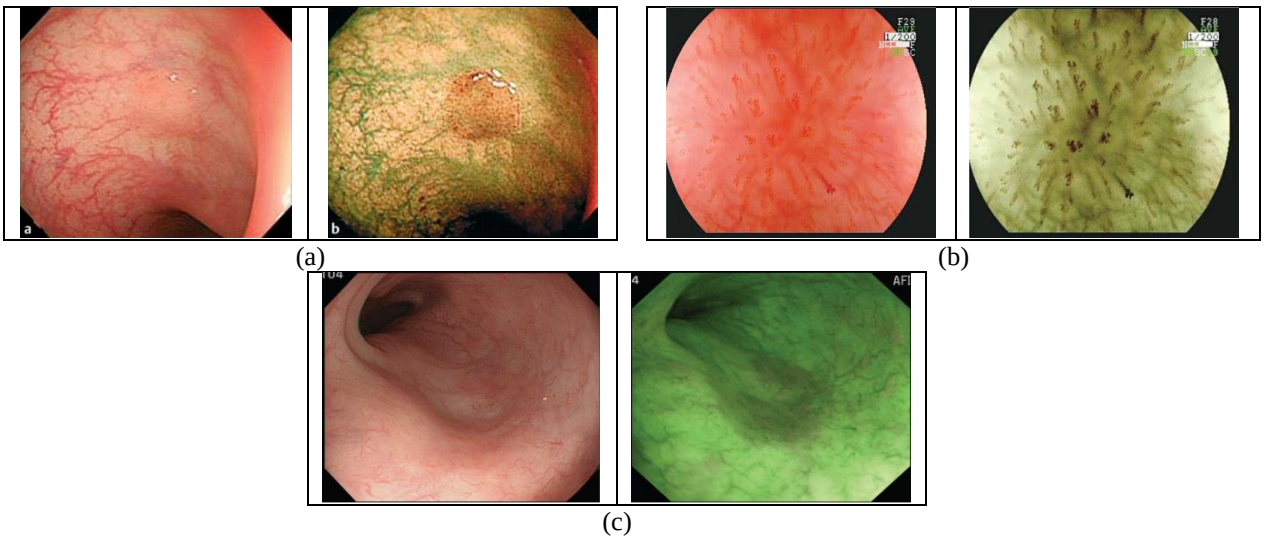


Fig. 1.1 Comparison between (a) WLI and NBI, (b) WLI and CE, and (c) WLI and AFI

## 1.3 Motivations

It is shown that WCE endoscopic images are often dark and unclear. Several gastroenterologists commented that the WCE images are often not clear enough to see the mucosa structure of the digestive tract compared with traditional endoscope [10] [12] [13]. However, even when traditional endoscope is practiced, the gastroenterologists continue to face

difficulty when identifying mucosa structures, pit patterns, tissue and vascular characteristics of GI tract in the images [18] [14] [15] [16] [17] [19]. Endoscopic images suffer from various degradations, such as low image quality of CMOS image sensor, non-uniform brightness and poor contrast [6] [7] [12] [13]. As a result, the image quality is greatly degraded making it difficult to detect and identify all important features of GI tract. This situation also poses challenges to computer aided detection (CAD) such as bleeding regions, tumour and defected polyp detection etc. To overcome this situation and facilitate the detection accuracy, it is necessary to enhance the features of endoscopic images [20].

The key focus in this research is to establish post-processing algorithms that can greatly enhance and highlight the features of endoscopic images. The features we target are: mucosal surface and structures, pit pattern, size and pattern of micro-vessels, tissue and vascular characteristics, superficial layer of mucosal and abnormal growths. The status of gastric glands and pits can be analyzed by mucosal surface and structures [21]. The quality of the lesion and depth invasion can be understood by diagnosing pit pattern [22]. Early stage of cancer can be detected by following the status of tissue and vascular characterization [23]. Furthermore, abnormal growths can be identified through the detection of color abnormalities in the endoscopic images. The enhancement of the above mentioned features can greatly improve early detection and diagnosis of GI diseases.

In this research work, two post-processing techniques for endoscopic images are proposed. The techniques have different approaches for image enhancement. The first technique enhances color images with strong contrasts. It can also enhance grayscale images and reproduce color from a theme image collected from the same or similar physical location of the GI tract.

The second technique can only enhance color endoscopic images, which reproduces pseudo color that is similar to the color reproduced by CE, NBI and AFI techniques.

## 1.4 Thesis objectives

The key challenge of developing endoscopic color image enhancement method is to enhance and highlight the main features of the endoscopic images without introducing any artificial color information and adding distortion to existing features. Considering the previous works and application demands, the following research objectives are set:

- To develop color image enhancement methods that can enhance and highlight key features of endoscopic images.
- To develop a color reproduction algorithm for reproducing strong original or pseudo color contrast which can highlight mucosal structure and abnormalities.
- To measure the quality of the proposed technique with respect to contrast enhancement, edge enhancement, color enhancement and color distortion.
- To compare the performance of the proposed techniques with other related works.

## 1.5 Thesis organization

The thesis is structured in seven chapters. The brief descriptions of each of the chapters are given below.

Chapter 1: *Introduction* presents the overview of endoscopic systems, endoscopic imaging, motivation, and thesis organization.

Chapter 2: *Endoscopic imaging techniques* discusses the related literatures on both in-chip and post-processing techniques for endoscopic image enhancement along with their limitations.

Chapter 3: *Endoscopic image enhancement based on adaptive sigmoid function and space-variant color reproduction (ASSVCR)* introduces the first technique for enhancing endoscopic images. It consists of two stages: adaptive sigmoid function based image enhancement and space-variant chrominance mapping color reproduction. The adaptive sigmoid function based grayscale enhancement is discussed in the *Image enhancement* section. The space variant color reproduction is demonstrated in the *Color reproduction* section.

Chapter 4: *Tri-scan technology for endoscopic image enhancement* introduces the second technique. Here, the color image enhancement is done in three stages and each stage is briefly discussed in the following section: *Tissue and surface enhancement, Mucosa layer enhancement* and *Color tone enhancement*.

Chapter 5: *Result and Discussion* demonstrates the visual assessment of proposed techniques. It also presents a comparative analysis between two techniques.

Chapter 6: *Performance Analysis* presents the objective evaluation of the proposed techniques. Both techniques are evaluated using several performance metrics such as focus value, statistic of visual representation, measurement of uniform distribution, color similarity test, color enhancement factor (CEF) and time complexity with other related works. Finally, the performance analysis between two techniques is also presented.

Chapter 7: *Conclusion and Future Work* presents the summary and discussion of this research work, and also presents topics for future developments.

# Chapter 2: Endoscopic imaging techniques

Color Image enhancement plays a major role in diagnosis by gastrointestinal endoscopy [8]. Many GI diseases can be prevented and cured if detected early. Different features of endoscopic images help gastroenterologist predict disease symptoms. There are few endoscopic imaging techniques that can enhance and highlight certain features of the endoscopic images. There are also some digital imaging algorithms, which are popular in enhancing the features of endoscopic images. These imaging techniques are divided into two categories: In-chip techniques and Post-processing techniques.

## 2.1 In-Chip techniques

The popular in-chip endoscopic imaging techniques are Narrow band imaging (NBI) [18] and Auto-florescence imaging (AFI) [14]. Though the image acquisition processes in both cases are similar, they differ from light sources and wavelengths of the filters used. These imaging techniques are briefly discussed below.

### *2.1.1 Narrow band imaging (NBI)*

The NBI technology uses narrow light sources to enhance visualization of the surface micro-vessels [18]. There are two types of NBI systems. In the NBI of the RGB sequential illumination system, narrow spectra of the red, green, and blue light that are centered on 415 nm, 445 nm, and 500 nm are used [8]. In the NBI of the color chip system, a single filter with a 2-band pass characteristic is used to generate the NBI images. The filter has narrow bandwidths of central wavelengths at 415 nm (blue) and 540 nm (green) [8]. On the endoscopy monitor, the signals obtained from the two specialized filters are combined to form a pseudo color image. These shorter wavelengths of light permit focused visualization of micro-vessels of the superficial layer of the mucosa and sub-mucosa. As the hemoglobin absorbs these optimized

wavelengths of light, NBI can provide the detailed characterization of lesions. It can also aid the gastroenterologist in the differentiation of abnormal mucosa from normal, because the pattern and size of the micro-vessels in the mucosa and sub-mucosa change when tissue becomes metaplastic, dysplastic, and neoplastic. Fig.2.1 presents some examples of WLI and their corresponding NBI images.

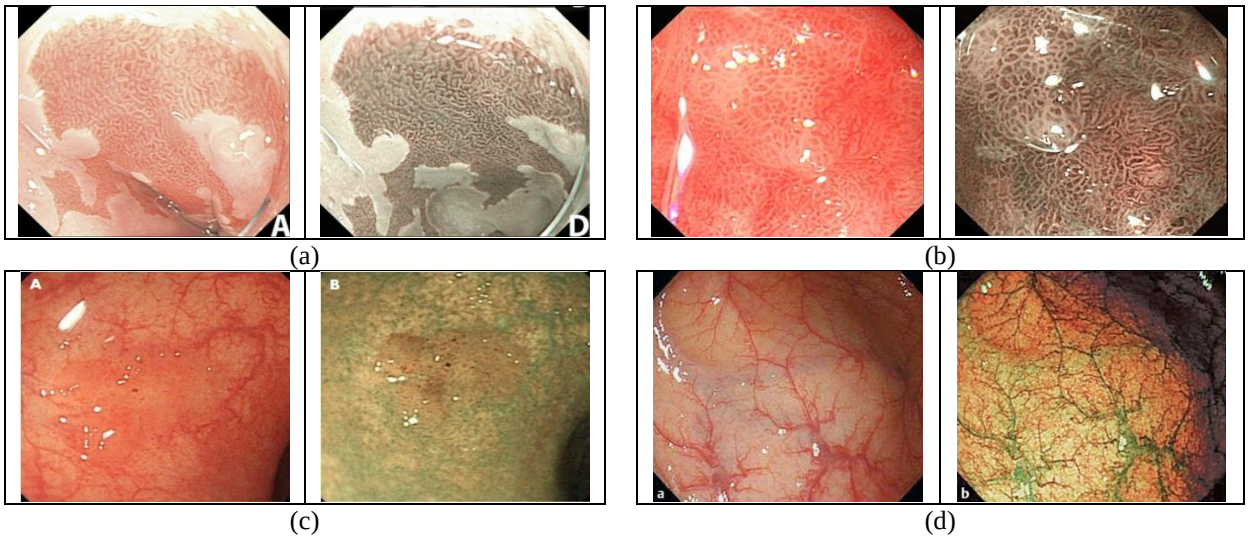


(a) (b) (c) (d)

Fig. 2.1 A typical example of four WLI endoscopic images and their corresponding NBI images

Several researchers concluded that NBI appears to be a less time-consuming but with higher miss rate [16] [19]. Additionally, it doesn't improve the adenoma detection or reduce miss rates during screening colonoscopy. No difference has been observed in the diagnostic efficacy of NBI system [16] [17].

### *2.1.2 Autofluorescence imaging (AFI)*

AFI is based on the principle that certain endogenous substances, such as nicotinamide, adenine dinucleotide, flavin adenine dinucleotide, collagen and endogenous fluorophores, emit fluorescent light when excited with short wavelengths of light [14]. In AFI, a special rotating color filter wheel in front of the xenon light source sequentially generates blue light (390-470nm) and green light (540–560nm) for tissue illumination [8]. In front of the CCD camera, an interference filter is placed to block the blue light excitation. This filter enables tissue

autofluorescenece at range of 500-630nm; thus, the reflected green light filters through. The sequentially captured images of autofluorescence and green reflectance are incorporated into a real-time pseudo color image by a processor. In the pseudo color AFI image, normal or non-dysplastic mucosa typically appears green and dysplastic tissue appears dark purple. Fig. 2.2 presents some examples of typical WLI and their corresponding AFI images.

Though AFI highlights the non-dysplastic and dysplastic tissue in mucosa surface, it doesn't substantially impact the overall diagnosis of neoplasia [24] [25] [26]. Furthermore, the false-positive ratio and the number of unnecessary biopsies are also likely to increase. On per lesion basis, AFI shows the highest false positive rate [25]. In short, lesions identified with AFI rarely contain more advanced stages of neoplasis.

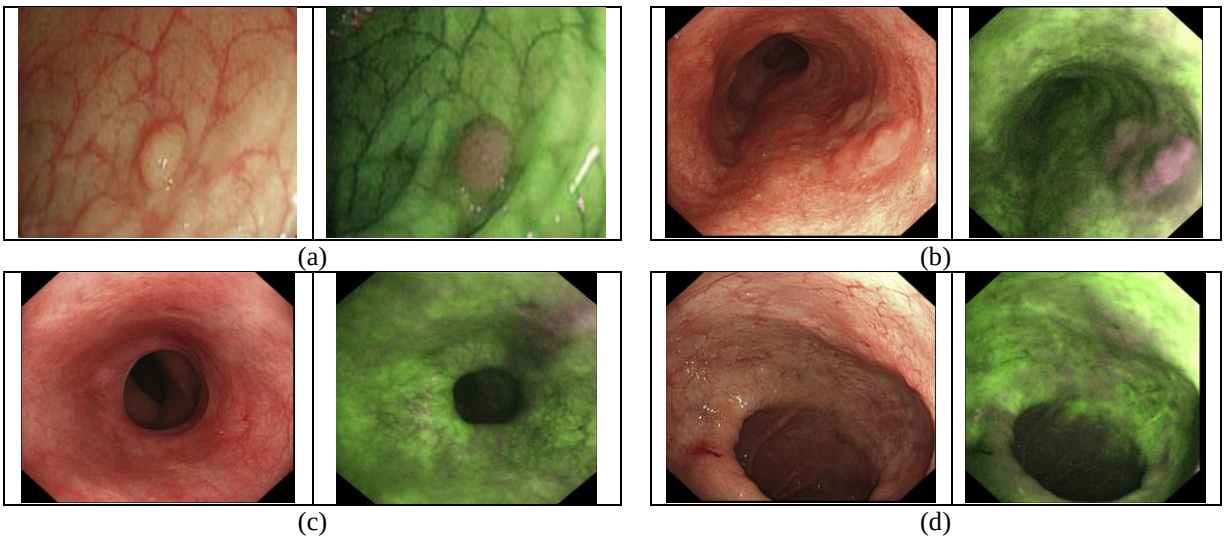

Fig. 2.2 A typical example of four WLI endoscopic images and their corresponding AFI images

## 2.2 Post-processing techniques

The popular post-processing techniques are divided into three sections: virtual chromoendoscopy, image enhancement and color reproduction. Virtual chromoendoscopy introduces a newly developed post-processing system for endoscopic image enhancement that is known as Fuji Intelligent Color Enhancement (FICE) [13]. Image enhancement presents other

related post-processing techniques that have been used for enhancing endoscopic images. Color reproduction presents different colorization techniques that can reproduce original or pseudo color with strong contrast. These techniques are briefly discussed below:

### *2.2.1 Virtual chromoendoscopy*

Fuji Intelligent Color Enhancement (FICE) [27], a recently developed virtual chromoendoscopy system, can simulate an infinite number of wavelengths in real time. Briefly, the software applies an algorithm to real-time endoscopic image, which is deconstructed to determine a wavelength for each of the three colors (red, green, blue). The image is instantaneously reconstructed after changing the wavelengths. The penetration of light actually varies with wavelengths. For example, those in the range of 400-500 nm are ideal for analyzing surface structure. Whereas, longer wavelengths of about 550 nm are more effective for visualizing blood vessels, due to the absorption properties of hemoglobin. Moreover, it is possible to create many reconstructed images using an infinite number of wavelength combinations. Fig. 2.3 presents some examples of WLI and their corresponding FICE images. Not all the combinations of wavelength channels can enhance the subtle features of mucosal layer and structure [15]. The combinations of different wavelength channels differ based on the position of GI tract. Similar to NBI, FICE appears to be less time consuming with a higher miss rate [17] [27]. FICE doesn't improve the detection of small polyp histology during screening colonoscopy, but it can be improved using magnified endoscopy [19]. Moreover, it doesn't improve the abdomen detection [27].

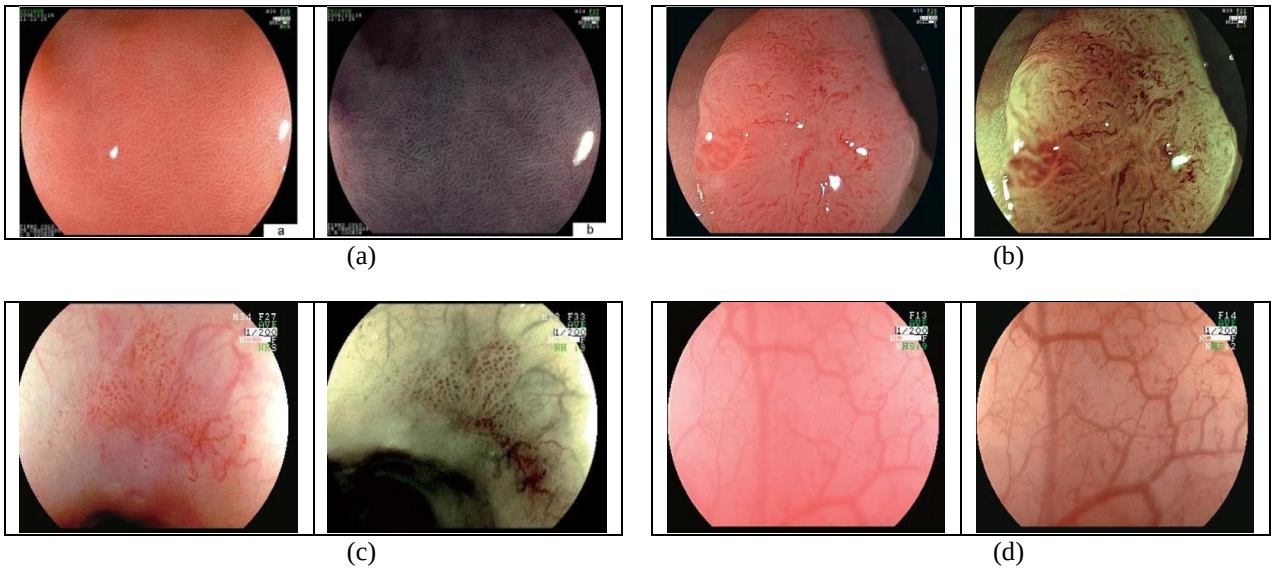

Fig. 2.3 A typical example of four WLI endoscopic images and their corresponding FICE images

### *2.2.2 Image enhancement*

Image enhancement presents some other global and adaptive image processing techniques to overcome inhomogeneous or non-uniform brightness and poor color contrast problems, such as adaptive histogram equalization (AHE) [28], contrast-limited adaptive histogram equalization (CLAHE) [29], high boost filtering (HBF) [30], and brightness preserving dynamic fuzzy histogram equalization (BPDFHE) [31]. They can be applied on both grayscale and color endoscopic images. If these techniques are applied on the grayscale images, then color reproduction is required to retrieve the original color with contrast.

AHE applies locally varying grayscale transformation to each small block of the image, thus requiring the determination of the block size [32]. Instead of focusing on the entire image, CLAHE operates on small regions in the image, often called tiles, which are based on user assigned parameters. Finally, the neighboring tiles are combined using bilinear interpolation to eliminate artificial included boundaries. Two drawbacks of this technique are noise enhancement in smooth regions and image dependency of the contrast gain limit [32]. HBF emphasizes high frequency components without eliminating the low frequency. It may add distortions to the

smoothing regions due to over-filtering. BPDFHE is the modification of the brightness preserving dynamic histogram equalization (BPDHE) [33] that preserves the brightness and improves contrast enhancement abilities, while reducing its computational complexity. However, BPDFHE introduces additional artifacts depending on the variation of gray level distribution [34] which may lead to inaccurate diagnosis.

### *2.2.3 Color reproduction*

There are different color reproduction methods that can subsequently differentiate the features and abnormalities by adding real or pseudo color in an image. In [35], the color information is assigned to each pixel in the gray image by matching each grayscale image, pixel to a pixel, in the target swatch, using Euclidean distance. Here, the swatches are used to guide the matching process. The algorithm suffers from high computational complexity and processing time. Additionally, it introduces artifacts, which may effect the diagnosis accuracy. In another work [36], the authors have used a set of seed points and their respective color vectors in the RGB format with a YUV-based classification. In [37], a quadratic objective function-based optimization method is used to interpolate the U and V components of the YUV color space over the entire image, using a set of color scribble lines. In [38], pseudo colors are employed to colorize grayscale images, using different $64 \times 3$ color matrices. It does not reproduce a visually appealing color on the entire image and introduces blurriness on the high contrast edges. None of the above-mentioned methods have ever been applied to endoscopic imaging. In a recent work by our group, a color enhancement scheme is presented that is dedicated to enhance endoscopic images [39] [40] [41]. In [39] and [40], a color reproduction scheme based on the neighborhood statistic method is used to reproduce the color from a theme image to grayscale endoscopic image. Here, the chromaticity information has been transferred to chrominance planes by matching luminance and texture information between images. The overall color contrast is

somewhat increases but suffers from high computational complexity. In [41], a space variant color reproduction is done by generating a real color map by transferring and modifying old chrominance values either from theme image or input image.

These in-chip and post-processing techniques are used in endoscopic images for enhancing and highlighting the subtle features of mucosal layer and structure. Still these techniques have limitations and often cannot enhance the subtle features. Some of them may add artificial artifacts and noise, which can mislead the diagnostic decision. That’s why, new techniques are constantly developed.

# Chapter 3: Endoscopic image enhancement based on adaptive sigmoid function and space-variant color reproduction

This chapter presents an endoscopic image enhancement technique based on adaptive sigmoid function and space-variant color reproduction (ASSVCR). It can enhance the texture information of endoscopic images and highlight pit patterns, mucosal surfaces and structures, defected polyps, tissue and vascular characterizations of GI tract. It consists of two stages: adaptive sigmoid function based image enhancement and space-variant chrominance mapping based color reproduction. The image enhancement is done on the luminance plane, and later in the process, the chrominance planes are used to reproduce strong color contrast. The block diagram of ASSVCR is shown in Fig. 3.1. The stages are briefly discussed below.

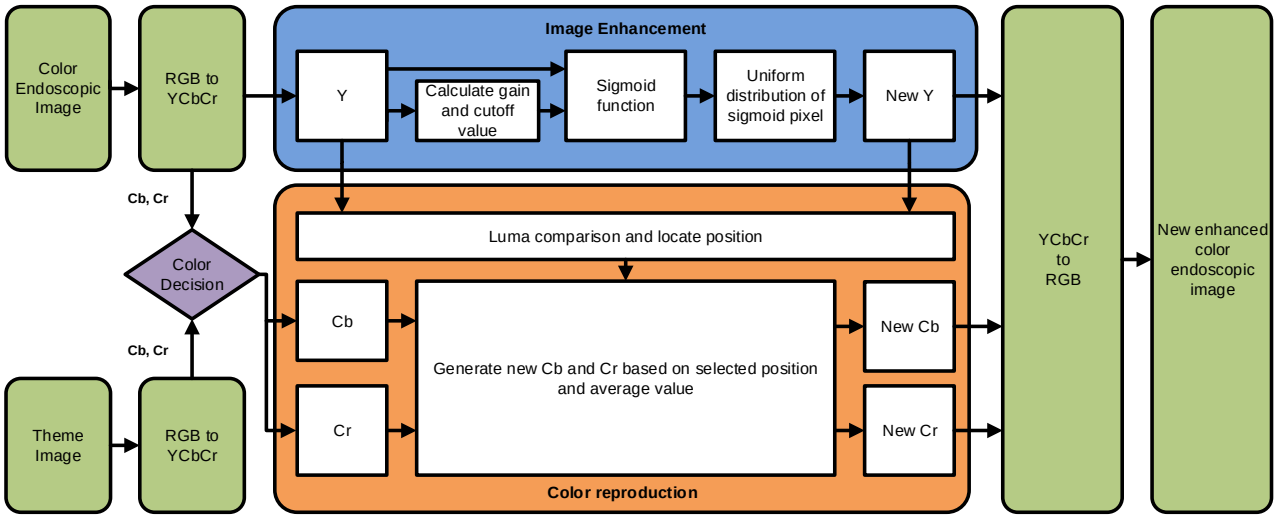


Fig. 3.1 Block diagram of ASSVCR

## 3.1 Image enhancement

At first, the color endoscopic image is converted into $YC_bC_r$ color space using (3.1). Here, $Y$ is luminance or luma, and $C_b$ and $C_r$ are chrominance components. The color space conversion provides the opportunity to process different luma pixels for enhancement and chrominance pixels for color reproduction.

$$\begin{bmatrix} Y \\ C_b \\ C_r \end{bmatrix} = \begin{bmatrix} 0.257 & 0.504 & 0.098 \\ -0.148 & -0.291 & 0.439 \\ 0.439 & -0.368 & -0.071 \end{bmatrix} \begin{bmatrix} R \\ G \\ B \end{bmatrix} + \begin{bmatrix} 16 \\ 128 \\ 128 \end{bmatrix} \quad (3.1)$$

Here, $Y$ represents grayscale image. After conversion, the ASSVCR normalizes grayscale image and each chrominance plane between 0 – 1 using (3.2).

$$Y_{norm}(Y) = \frac{Y - Y_{\min}}{Y_{\max}} \quad (3.2)$$

Here, $Y_{\min}$ and $Y_{\max}$ are the minimum and maximum pixel values. Later, the normalized grayscale image is enhanced using adaptive sigmoid function and uniform distribution.

### *3.1.1 Adaptive sigmoid function*

The proposed technique uses contrast manipulation procedure for image enhancement. Generally, contrast manipulation can be done either globally or adaptively. Global techniques apply a transformation to all image pixels, while adaptive techniques use an input-output transformation that varies adaptively with local image characteristics. The proposed ASSVCR technique transforms the pixel values adaptively using sigmoid function.

In general, a sigmoid function is real value and differentiable, having either a non-negative or non-positive first derivative that is bell shaped. It has been used in a variety of researches that is related to image processing [42] [43] [44]. Using $x$ for the input, the sigmoid function is given below:

$$f(x) = \frac{1}{(1 + e^{-x})} \quad (3.3)$$

During the experiment, we have observed that in a certain exponent, some tissue and vascular characteristics as well as some mucosa structures are highlighted, which are not clearly visible in the original image. To control the exponent, we have introduced two coefficients in the

sigmoid function. Using $x$ for the input, $g$ for gain and $k$ for cut-off, the modified sigmoid function is expressed below:

$$f(x) = \frac{1}{(1+e^{g(k-x)})} \tag{3.4}$$

The cut-off value determines the midpoint of the input curve, and the gain controls the amount of bending. These two parameters give us the control to train the proposed technique to generate a certain exponent that highlights some vascular characteristics. Let, $x = 0, 0.1, 0.2, \ldots, 1$ normalized image pixel values where sigmoid function (3.4) is applied. Fig. 3.2 presents the sigmoid curve of input pixel values based on different cut-off and gain.

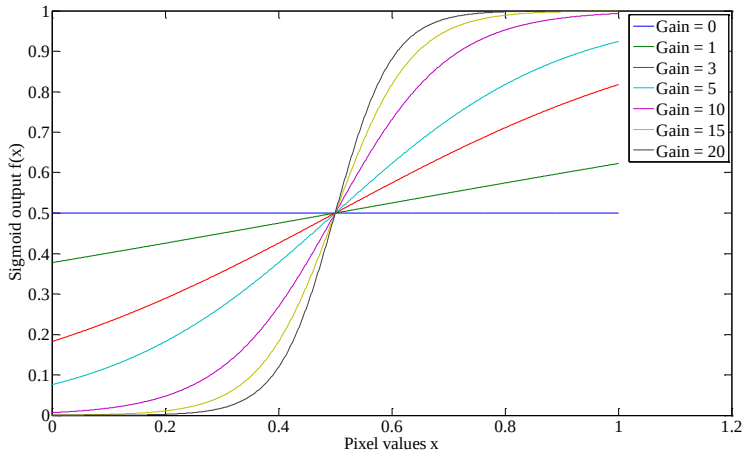


(a)

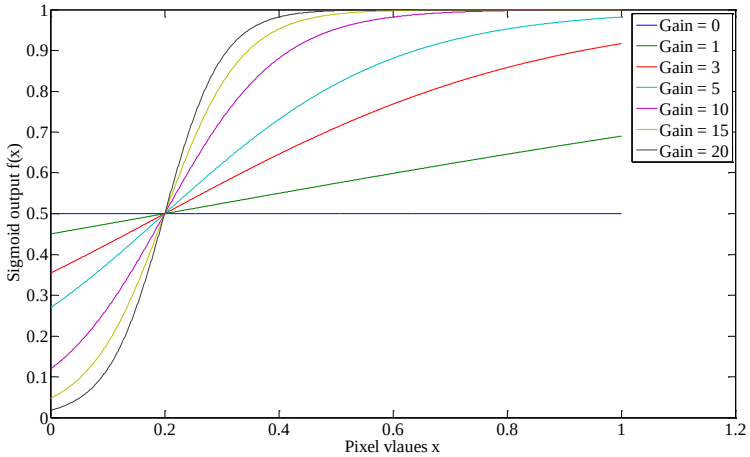


(b)

Fig. 3.2 Sigmoid effect on pixel for different gain values (a) with 0.5 cutoff; (b) with 0.2 cutoff

These parameters (gain and cut-off) can control the overall brightness and contrast level of the image too. The cut-off value controls the amount of brightness, and the gain controls the consecutive difference between pixels. To maintain the exponent into target range, we have proposed algorithms to generate cut-off and gain value. Based on the input pixel values, equation (3.5) and (3.6) generate specific cut-off and gain value. Later on, these values are used in (3.4) to generate the sigmoid image.

$$k = \frac{\sum_{i=1}^{n} x_i}{n} \tag{3.5}$$

$$g = A \times \log(\frac{S_m}{S_n}) \times \frac{\sum_{i=1}^{n} x_i}{n} \tag{3.6}$$

Where, $A = 100$, $S_m = 6$, $S_n = 5$, $x_i$ is the pixel values of $i^{th}$ position and $n$ is the number of pixel. These values are heuristically collected from simulation mode. These values produce the desired exponent that highlights the subtle tissue and vascular characteristics as well as mucosa structures in the endoscopic images. Later, these values are used in (3.4) to generate the sigmoid image. Fig. 3.3 shows the original images with the corresponding adaptive sigmoid images. Here, it can be observed that some vascular characteristics and mucosa structures are highlighted in the sigmoid images.

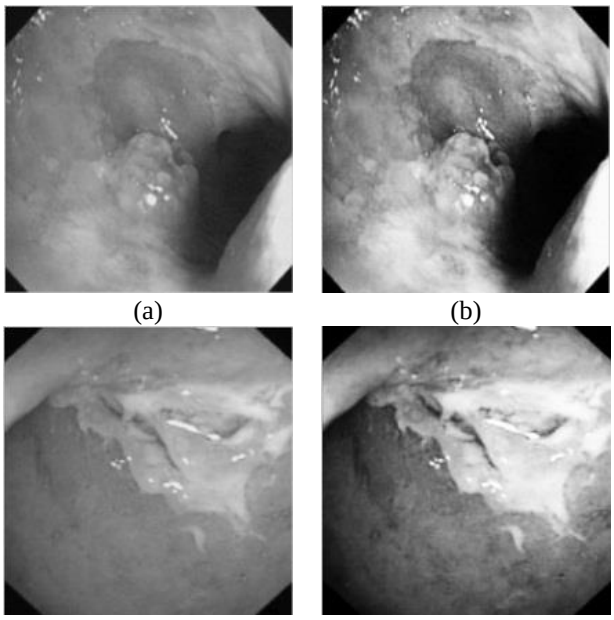

(a) (b)

(c) (d)

Fig. 3.3(a) and (c) Original images; (b) and (d) Adaptive sigmoid images

### *3.1.2 Uniform distribution of sigmoid pixels*

In the next stage, the sigmoid pixels are uniformly distributed to increase the contrast level. It helps to visualize the vascular characteristic of the darker part of an adaptive sigmoid image. It also highlights the pit patterns, defected polys or abnormal growths in the images. It is employed by effectively spreading out the most frequent intensities.

Let, $f$ be a given sigmoid image represented as $i$ by $j$ matrix of integer pixel intensities ranging from 0 to 255. Let, $p$ denote the normalized histogram of $f$ with bin for possible intensities. So,

$$\boldsymbol{p_m} = \frac{\textbf{\textit{Number of pixels with intensity m}}}{\textbf{\textit{total number of pixels}}} \tag{3.7}$$

Where, $m = 0,1,2,...,255$. The uniformly distributed sigmoid image $\Psi$ is defined as,

$$\Psi_{i,j} = floor((L-1)\sum_{n=0}^{f_{i,j}} p_m) \tag{3.8}$$

Where, $floor()$ rounds up the pixel value to the nearest integer. Normally, the cumulative distribution function (CDF) of an image does not form a straight line implying that the pixel

values are not equally likely to occur. In the proposed technique, the uniform distribution of sigmoid pixels is done by flattening the CDF using (3.7) and (3.8). Fig. 3.4 shows the visual comparison of uniform distribution of sigmoid pixels.

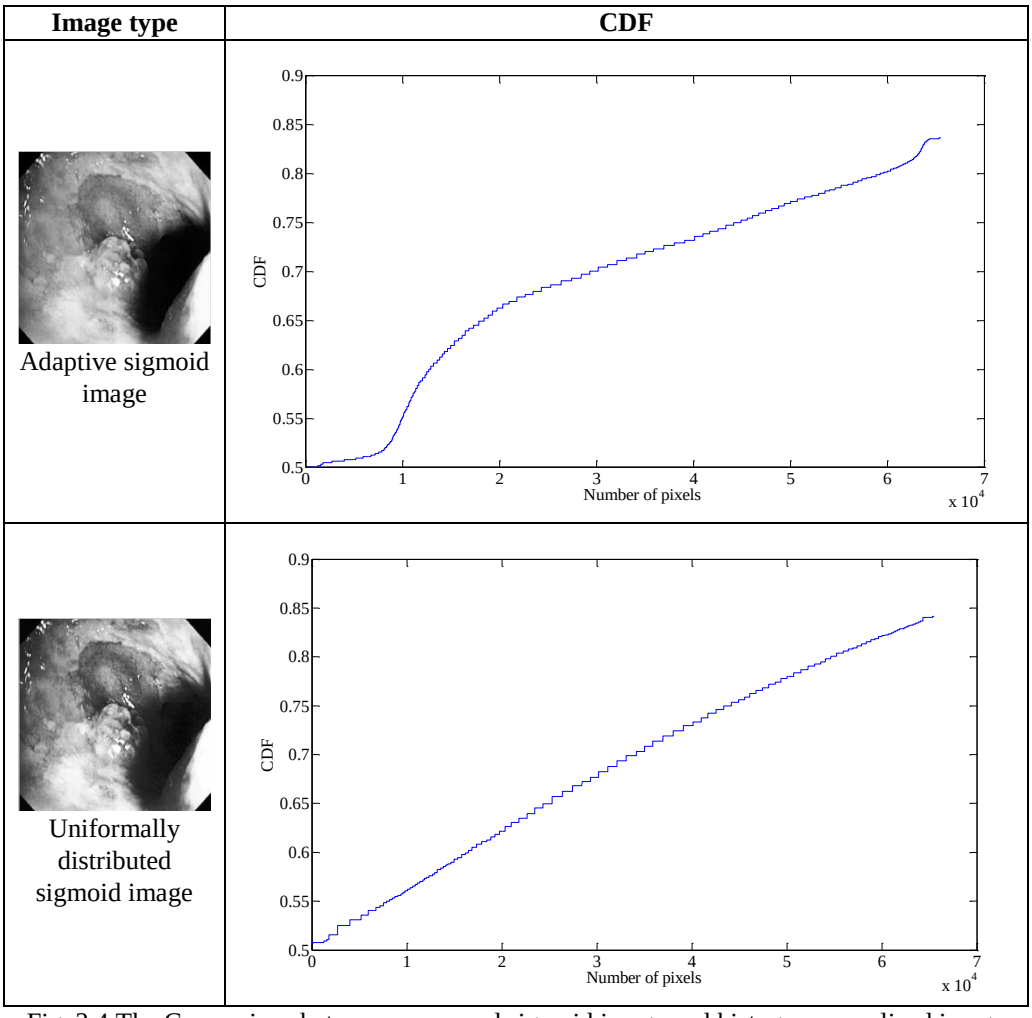


Fig. 3.4 The Comparison between processed sigmoid image and histogram equalized image

Here, it is clearly visible that the CDFs of the uniformly distributed sigmoid images are flattened. It also highlights the infected area surrounding the polyp (e.g. abnormal growths) and pit patterns. Later on, this uniformly distributed sigmoid image $\Psi_{i,j}$ is treated as new enhanced grayscale image ($\Psi$).

## 3.2 Color reproduction

In the second stage of the proposed ASSVCR technique, we apply color reproduction. It is a computer-assisted process of adding color to a monochrome image [45] [46]. Using the proposed technique, it is possible to retrieve the original color with a better tone or to add pseudo color using a theme image. This choice is controlled by the user through the "color decision" module (see Fig. 3.1), which selects the chrominance components.

**Case 1:** To retrieve the original color, the new $C_b$ and $C_r$ planes are created by matching the original $C_b$ and $C_r$ values to corresponding Y pixels from the original grayscale image. First of all, the positions of all $C_b$ and $C_r$ values in the plane for a particular Y pixel are identified as expressed by (3.9):

$$[m,n] = locate(Y \quad - Y_{i,j}) \tag{3.9}$$

Here, $Y$ is normalized grayscale image, $Y_{i,j}$ is a pixel of normalized grayscale image and $[m,n]$ holds one or multiple positions. These positions will allow us to generate new chrominance planes. Two scenarios may occur: (a) if only one chrominance value is found, it places that value in the corresponding positions in the new $C_b$ and $C_r$ planes. (b) Otherwise, if multiple chrominance values are found, it generates a new chrominance value using (3.10), and places it in the corresponding positions of the new $C_b$ and $C_r$ planes.

$$\bar{x} = \frac{\sum_{i=1}^{n} x_i}{n} \tag{3.10}$$

These steps continue until all pixels of the grayscale image are scanned. The new $C_b$ and $C_r$ will have the same dimension as the original grayscale image. Later, the enhanced grayscale image ($\Psi$), and the new $C_b$ and $C_r$ images are converted back to RGB image using (3.11).

$$\begin{bmatrix} R \\ G \\ B \end{bmatrix} = \begin{bmatrix} 1.164 & 0 & 1.596 \\ 1.164 & -0.392 & -0.813 \\ 1.164 & 2.017 & 0 \end{bmatrix} \begin{bmatrix} \psi - 16 \\ C_b^{new} - 128 \\ C_r^{new} - 128 \end{bmatrix} \tag{3.11}$$

**Case 2:** To add pseudo color, a theme image is required. It is applicable for only grayscale image (e.g. no color information is available). The selection of theme image is important as the color carries critical information of endoscopic images. The theme image must be selected from the same or similar physical location of GI tract. After selecting a proper theme color image, it is converted into $YC_bC_r$ space. Then, we create new $C_b$ and $C_r$ planes by matching the chrominance values of the theme image for the corresponding pixel ($\Psi_{i,j}$) of enhanced image. Here, the positions of all $C_b$ and $C_r$ values in the plane for a particular $\Psi$ pixel are identified as expressed by (3.12).

$$[m,n] = locate(Y_t - \Psi_{i,j}) \tag{3.12}$$

Here, $Y_t$ is a normalized theme grayscale image, $\Psi_{i,j}$ is a pixel of enhanced grayscale image and $[m,n]$ holds one or multiple locations. These locations allow us to generate the new chrominance plane with respect to the enhanced and theme grayscale images.

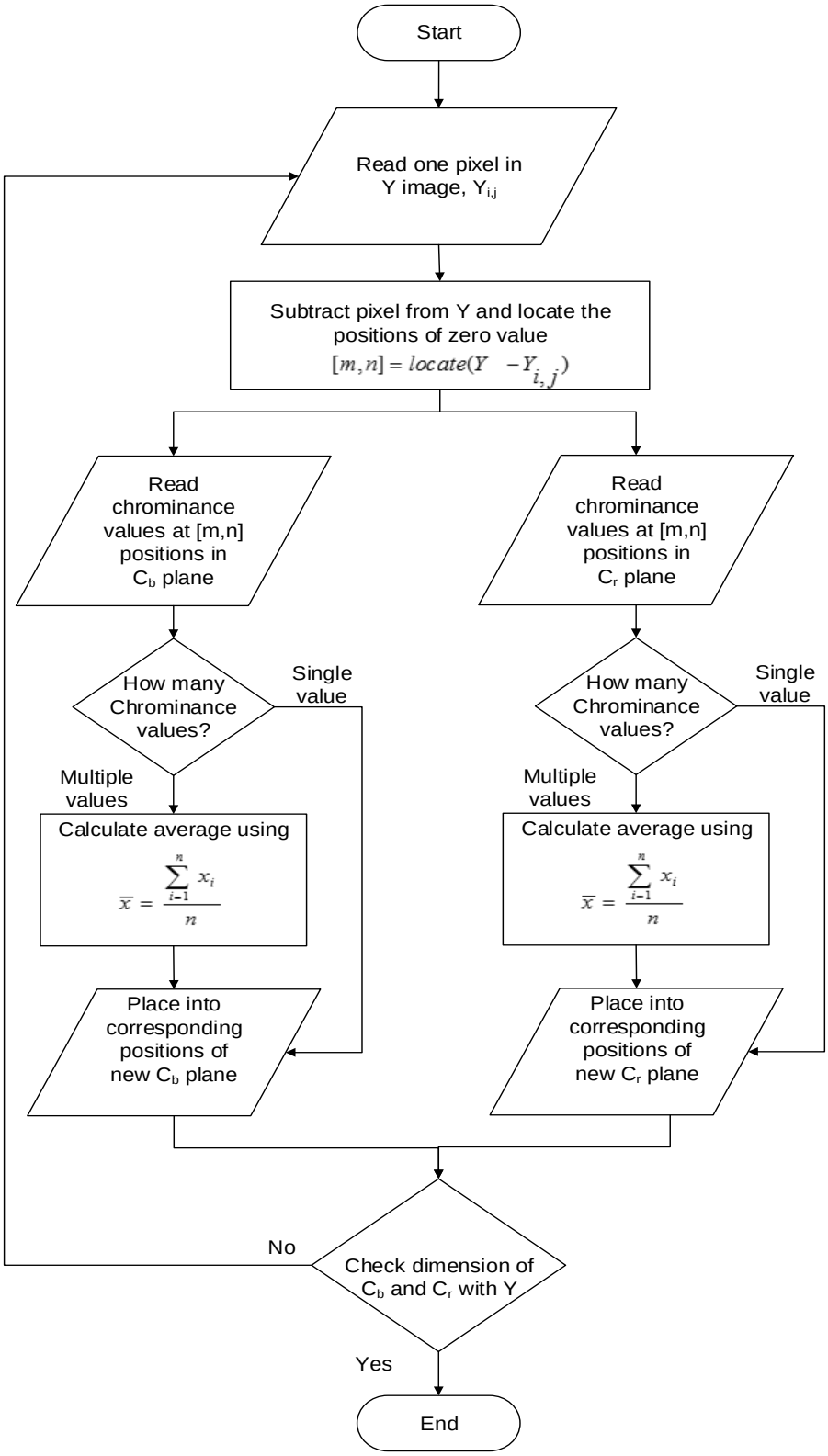


Fig. 3.5 Flow chart case 1: to retrieve original color

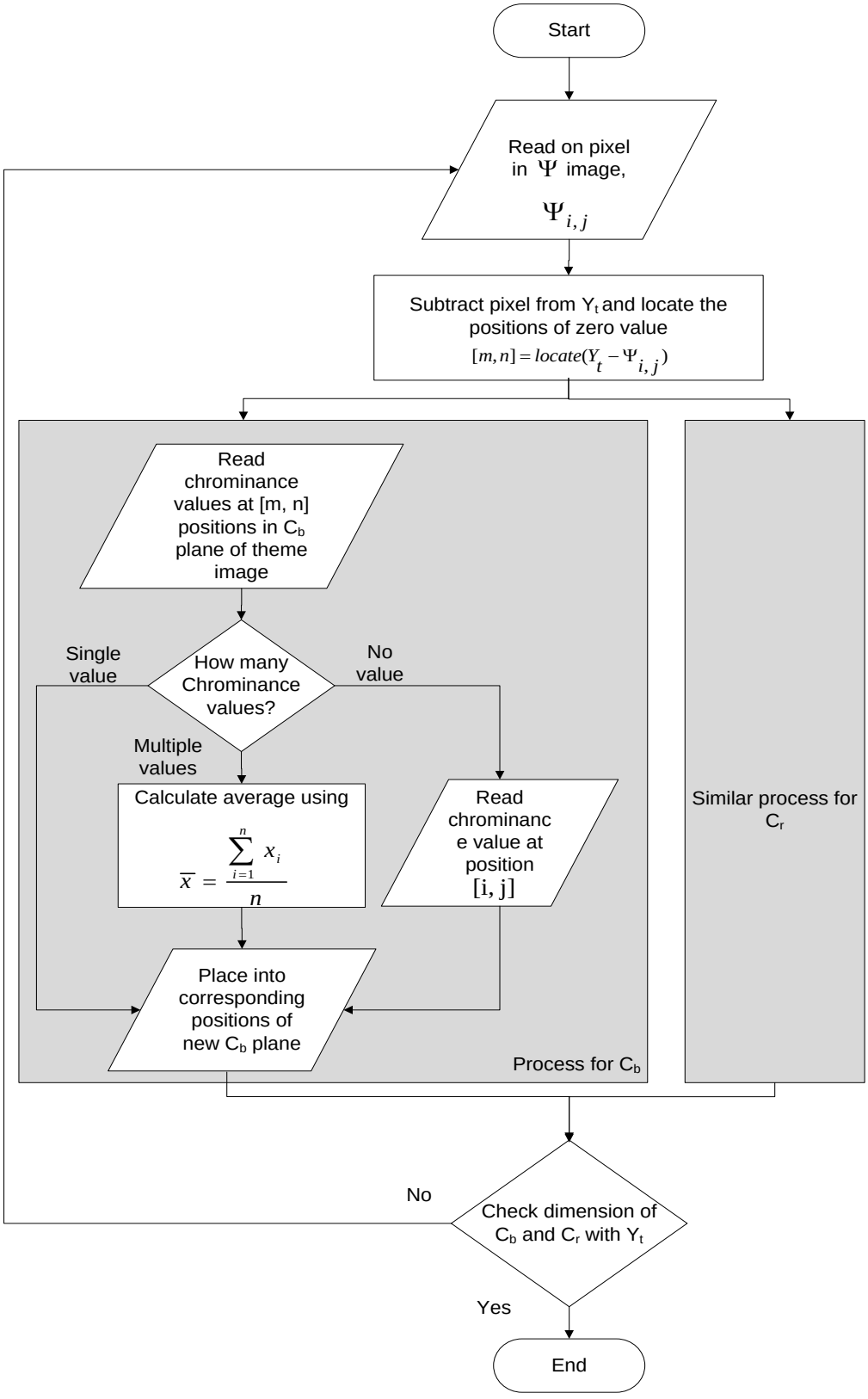


Fig. 3.6 Flow chart case 2: to add pseudo color from theme image

Three scenarios may occur: (a) if only one chrominance value is found, it places that value in the corresponding position in the new $C_b$ and $C_r$ planes. (b) if multiple chrominance values are found, it generates a new chrominance value using (3.10) and places it in the corresponding positions of the new $C_b$ and $C_r$ planes. (c) if no chrominance value is found, it reads the chrominance value with respect to the positions of $\Psi_{i,j}$ in theme image's $C_b$ and $C_r$ planes and places it in the corresponding position of the new $C_b$ and $C_r$ planes. These steps continue until all pixels of the enhanced grayscale image are scanned. The new $C_b$ and $C_r$ will have the same dimension of the original grayscale image. Later, the enhanced grayscale image ( $\Psi$ ) and the new $C_b$ and $C_r$ images are converted back to RGB image using (3.11).

In Fig. 3.5 and 3.6, the flow charts of the color reproduction algorithm are presented. Some reconstructed images for the two cases are shown in Fig. 3.7 and Fig. 3.8. It can be seen that the proposed ASSVCR technique reproduces original and theme color with strong contrast.

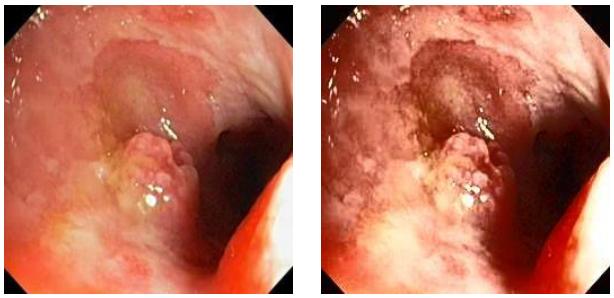

(a) (b)

Fig. 3.7(a) Original image and (b) enhanced image by the ASSVCR (color reproduced from original image)

(a) (b) (c)

Fig. 3.8(a) Original grayscale image (no color information is available) (b) enhanced color image by the ASSVCR (color reproduced from theme image shown in (c))

In summary, the proposed ASSVCR technique converts the color image into $YC_bC_R$ color space, applies adaptive sigmoid based image enhancement on the gray level, reproduces original color contrast using space-variant chrominance mapping based color reproduction, and converts the enhanced gray and new chrominance map into the RGB color space to generate an enhanced color endoscopic image. It enhances and highlights the tissue and vascular characteristics, mucosa structures, pit patterns and abnormal growths in the endoscopic image with strong color contrast.

# Chapter 4: Tri-scan technology for endoscopic image enhancement

This chapter presents the proposed tri-scan technique for enhancing and highlighting micro-vessels in superficial layers of mucosa, size and pattern of micro vessels, mucosa surfaces and structures, tissue and vascular characteristics, pit patterns and abnormal growths. Here, our main goal is to manipulate endoscopic RGB images, which are often unknown phosphor chromaticity. Basically, the RGB planes carry different spectral responses of the surface [47]. These spectral responses are mainly dependant on the camera sensor and its spectral sensitivity. From the observation of spectral sensitivities range of 300nm to 700nm of CMOS and CCD cameras and their effect on endoscopic images, it can be noticed that mostly R plane dominates higher wavelength regions, G plane dominates mid-wavelength regions and B plane dominates shorter wavelength regions. As a result, these individual spectral responses of R, G and B planes carry different spatial characteristics of endoscopic image. From Fig. 4.1, we can see the different spatial characteristics of R, G and B planes in an endoscopic image.

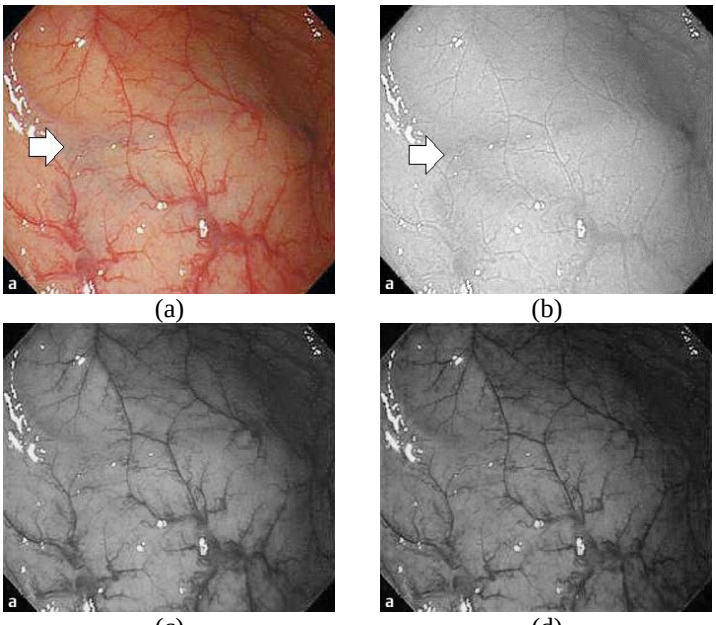

Fig. 4.1(a) Original RGB endoscopic image, and spatial characteristics of (b) R plane (c) G plane and (d) B plane

From Fig. 4.1, it can be noticeable that the G and B planes mostly carry the information of the mucosa structures, tissue and vascular characteristics and pit patterns. Here, only the edges and lesion borders are visible. On the other hand, the R plane carries the information related to the superficial layers of mucosa and pattern of micro vessels. In Fig. 4.1 image (a) and (b), the arrow sign indicates a superficial layer of mucosa, which is only visible in the R plane of the original color image. It is possible to highlight these subtle features, if these different spatial characteristics can be enhanced separately.

The proposed tri-scan technique performs enhancement in each plane to highlight the subtle features of endoscopic images. It consists of three stages: tissue and surface enhancement (TSE), mucosal layer enhancement (MLE) and color tone enhancement (CTE). The proposed tri-scan is shown in Fig. 4.2. A visual demonstration of the changes of spatial characteristics in each plane of the endoscopic image by tri-scan is also presented in Fig. 4.3. The stages are briefly discussed below.

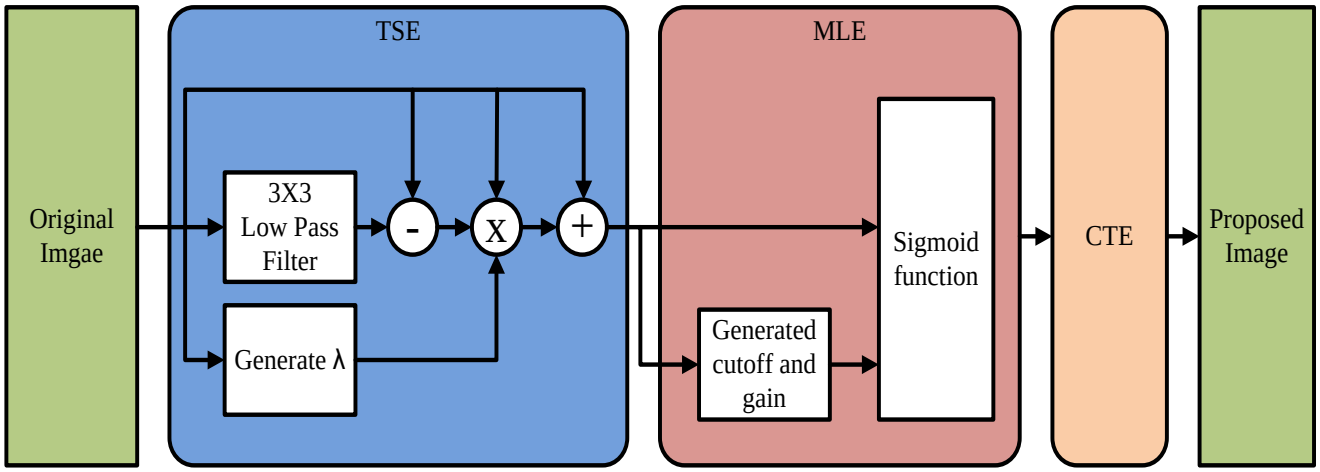


Fig. 4.2 Proposed tri-scan technology

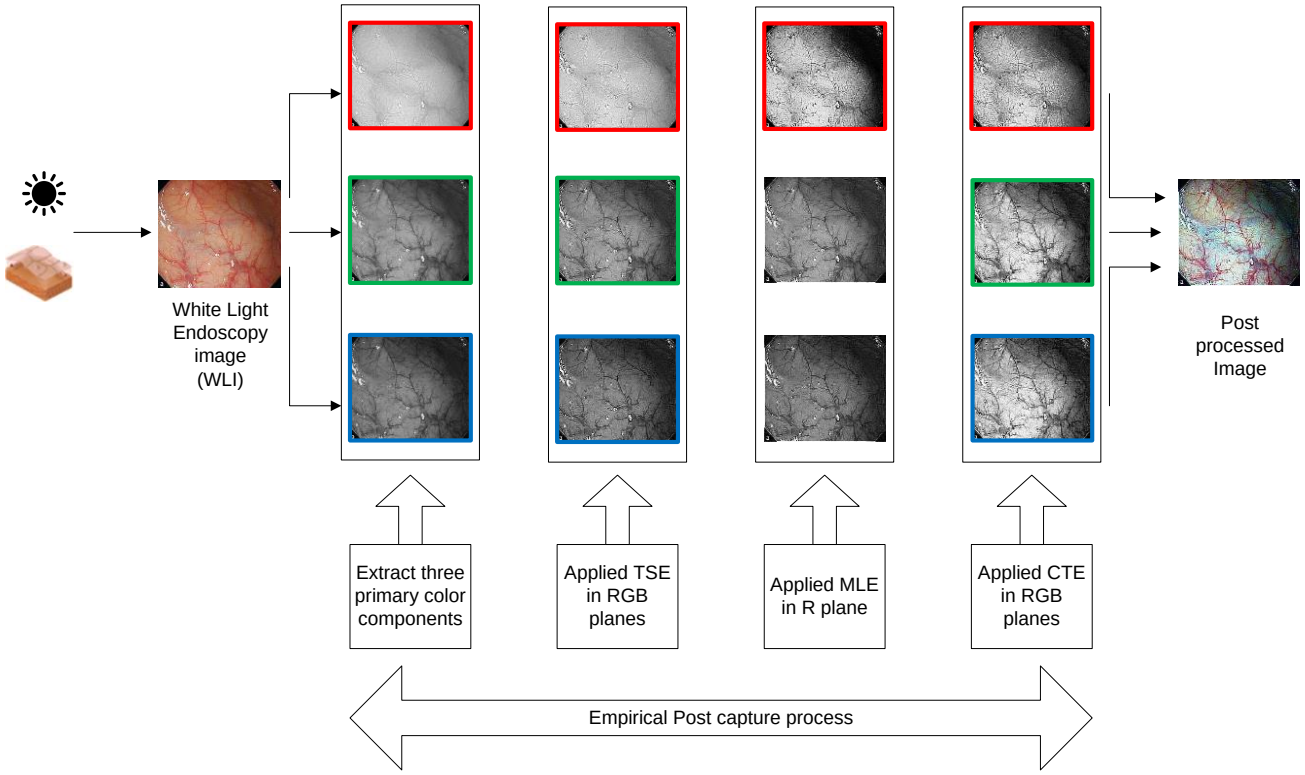


Fig. 4.3 A visual demonstration of the changes of spatial characteristics in each plane of the endoscopic image by proposed tri-scan technique

## 4.1 Tissue and surface enhancement (TSE)

At first, the color endoscopic image is divided into three primary color planes R, G and B. These color planes are normalized between 0 - 1 using (4.1). In TSE stage, each of these color planes will be treated as grayscale image.

$$N(x) = \frac{x - x_{\min}}{x_{\max}} \tag{4.1}$$

Here, the mucosa structure, tissue and vascular characteristics, and pit pattern in each plane are enhanced using modified linear unsharp masking. Traditionally, unsharp masking is a simple sharpening operator. It can enhance edges and other high frequency components, via a procedure that subtracts an unsharp or blurry version of an image from the original grayscale image [48]. At first, it produces an edge image $g(x, y)$ from an input image $f(x, y)$ using (4.2).

$$g(x,y) = f(x,y) - f_{blurry}(x,y) \quad (4.2)$$

Where, $f_{blurry}(x,y)$ is a blurry version of $f(x,y)$. Here, $3x3$ mean filter is used to produce the blurry image. Fig. 4.4 presents a $3x3$ mean filter, which is a simple sliding-window spatial filter that replaces the center value with a mean value of all the pixels in the window.

$$1/9 \times \begin{bmatrix} 1 & 1 & 1 \\ 1 & 1 & 1 \\ 1 & 1 & 1 \end{bmatrix}$$

Fig. 4.4 3x3 mean filter

The edge image carries all the high frequency components. These high frequency components are intensified by multiplying a sharpening factor $\lambda$ with the edge image. Finally, it is added to original grayscale image to produce the sharpened image using (4.3).

$$f_{sharpen}(x,y) = f(x,y) + \lambda \times g(x,y) \quad (4.3)$$

Here, $f_{sharpen}(x,y)$ is the sharpened image. The higher sharpening factor can produce more sharpened endoscopic images; however, at a certain level, it may introduce artificial artifacts. That's why, it is really important to control the sharpening factor based on the input pixels. Here, we have proposed an algorithm to control the sharpening factor using (4.4). It will keep the sharpening factor in a certain range so that no artificial information introduce.

$$\lambda = 10 \times \frac{\sum_{i=1}^{n} f(x,y)}{n} \quad (4.4)$$

Here, $n$ is the number of pixels. At first, $\lambda$ is generated from the input image $f(x, y)$ and used in (4.3) to generate sharpen image. The values in equation (4.4) are collected heuristically from the simulation mode.

The modified linear unsharp masking is employed in each plane of color endoscopic images to sharpen the edges and borders of mucosa surfaces, pit patterns and tissue and vascular characteristics. From Fig. 4.5, we can see the changes of tissue characteristics and mucosa structures between the original, blurry and sharpened color endoscopic images.

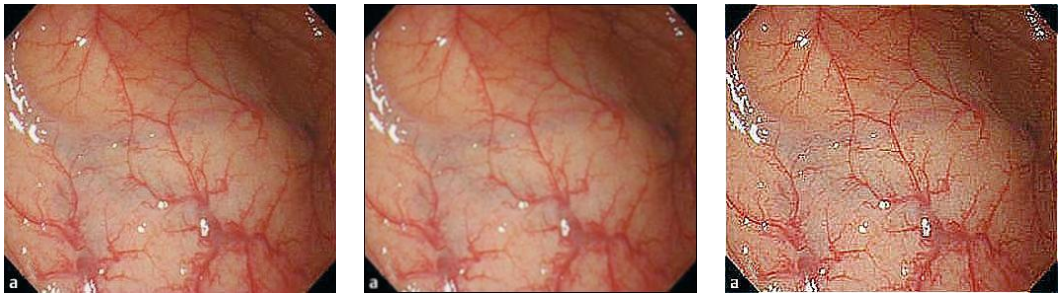

(a) (b) (c)

Fig. 4.5 (a) Original WLI endoscopic image, (b) blurry image and (c) TSE Sharpened image

## 4.2 Mucosa layer enhancement (MLE)

In MLE, the superficial layers of mucosa, and size and pattern of micro-vessels are enhanced and highlighted using contrast manipulation techniques. Here, we have used adaptive sigmoid (3.4) function to enhance these subtle features. As the R planes contain the spatial characteristics of superficial layers of mucosa, and size and pattern of micro-vessels (as previously mentioned), it is applied only on the R plane of sharpened color endoscopic image.

During the experiment, we have observed that in a certain exponent, some superficial layers of mucosa, and size and pattern of micro-vessels are highlighted, which are not clearly visible in the original image. This certain exponent is controlled by the two coefficients; cutoff ( $\kappa$ ) and gain ( $g$ ). The cut-off value determines the midpoint of the input curve, and the gain controls the amount of bending. These parameters (gain and cut-off) can also control the overall

brightness and contrast level of the input image. The cut-off value controls the amount of brightness, and the gain controls the consecutive difference between pixels. These two parameters give us the opportunity to control and train the proposed technique to generate a certain exponent that highlights those subtle features. Let, $x = 0,0.1,0.2,\ldots,1$ normalized image pixel values where sigmoid function (4.6) is applied. Fig. 4.6 present the sigmoid curve of input pixel values based on different cut-off and gain values, and the corresponding sigmoid images. Different combinations of gain and cut-off values generate different sigmoid images. In Fig. 4.6 (a) and (c), we can observe the changes of superficial layers of mucosa, which is previously mentioned in Fig. 4.1 using an arrow sign.

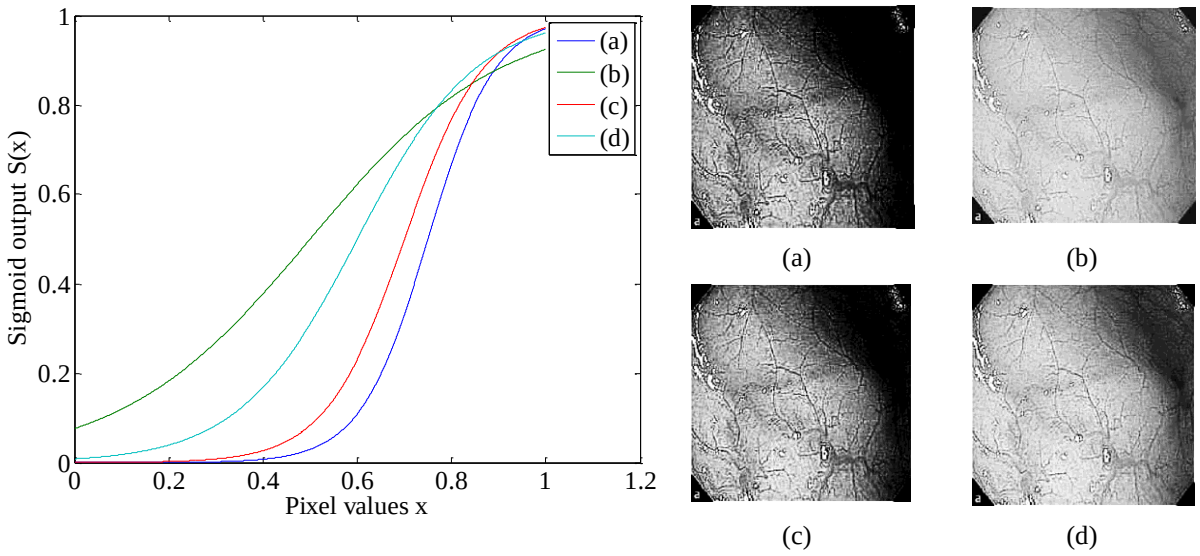


Fig. 4.6 Sigmoid effect on image (a) sigmoid image with 14 gain and 0.75 cutoff value (b) sigmoid image with 5 gain and 0.5 cutoff value (c) sigmoid image with 12 gain and 0.7 cutoff value (d) sigmoid image with 8 gain and 0.6 cutoff value

To maintain the exponent into the target range, we have proposed two algorithms to generate cut-off and gain values. Based on the input pixels, equation (4.5) and (4.6) generate specific cut-off and gain values. Later on, these values are used in (3.4) to generate the sigmoid pixels for R plane.

$$k = z + \frac{1}{2} * \left( \frac{\sum_{i=1}^{n} x_i}{n} \right) \tag{4.5}$$

$$g = \alpha \times \ln\left(\frac{\beta}{\sigma}\right) \times \frac{\sum_{i=1}^{n} x_i}{n} \tag{4.6}$$

Where, $z = 0.2, \alpha = 10,\ \beta = 23$ and $\sigma = 10$, $x_i$ is the input pixel values of $i^{th}$ position of R plane and $n$ is the number of pixels. These values are heuristically collected from simulation mode. In Fig. 4.7, we can see the difference of R plane between the TSE and MLE stage. The superficial layers of mucosa are better visible in the MLE stage compare to the TSE stage. The differences are also visible in the color endoscopic image as well.

## 4.3 Color tone enhancement (CTE)

In CTE stage, we have applied three dimensional (3-D) uniform distributions for modifying the pixels of R, G and B planes. The 3-D uniform distributions is accomplished by effectively spreading out the most frequent intensities. It eventually increases the contrast level and creates a different pseudo color background, which provides a better visualization of mucosa structures, pit patterns, superficial layers and abnormal growths.

Let, $f$ is a given image represented as $m$ by $n$ matrix of integer pixel intensities of three dimension ranging from 0 to $L-1$ . $L$ is the number of possible values that is 256. Let, $p$ denotes the normalized values of $f$ with bin for possible intensities. So,

$$\boldsymbol{P_n} = \frac{\textbf{\textit{Number of pixels with intensity n}}}{\textbf{\textit{total number of pixels}}} \tag{4.7}$$

Where, $n = 0,1,2,...,L-1$. Here it generates $P_n$ for all three dimensions. The 3-D uniform distribution can be expressed as,

$$\Psi_{r,g,b} = \begin{cases} floor((L_r - 1)\sum_{n=0}^{fr_{i,j}} p_{rn}), & R \quad plane \\ floor((L_g - 1)\sum_{n=0}^{fg_{i,j}} p_{gn}), & G \quad plane \\ floor((L_b - 1)\sum_{n=0}^{fb_{i,j}} p_{bn}), & B \quad plane \end{cases} \tag{4.8}$$

Where, $floor()$ rounds up the pixel values to the nearest integer.

In CTE stage, the 3-D uniform distribution creates light steel blue effect on the overall endoscopic image, thus increasing the visualization of the subtle mucosa structure, pit patterns, superficial layers and abnormal growths. It also employs indian red color effect on the tissue characteristics and mucosa structures, and royal blue effect on the superficial layer of mucosa. In Fig. 4.7 (CTE section), we can see the color effect on a typical endoscopic image. Here, we can easily identify the subtle features.

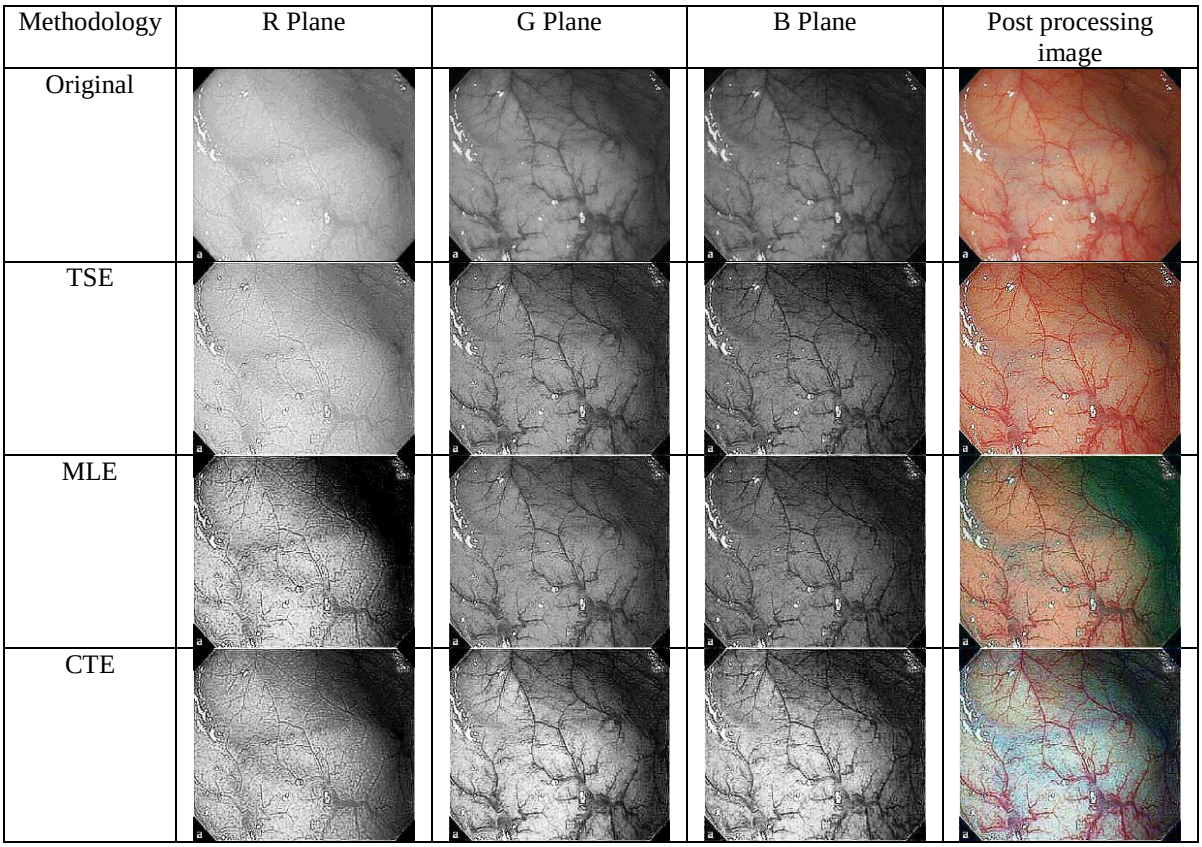


Fig. 4.7 A visual representation of the effect of proposed tri-scan on a typical endoscopic image

In summary, the proposed tri-scan enhances the endoscopic images into three stages. First, in the TSE stage, it sharpens the edges and borders of mucosa structures, and tissue and vascular characteristics using modified linear unsharp masking. Second, in the MLE stage, it enhances the superficial layers of mucosa, and size and pattern of micro-vessels in R plane using adaptive sigmoid function. Finally, in the CTE stage, it creates pseudo color effect on the overall endoscopic images using 3-D uniform distribution, which highlights and distinguishes the subtle features and abnormalities.

# Chapter 5: Result and discussion

This chapter presents the results and discussion of two proposed post-processing techniques. At first, the processed images using ASSVCR technique are presented and evaluated with respect to low contrast WLI images. Second, the processed images using tri-scan technique are shown and evaluated with other related works. Finally, a comparative analysis between two techniques is presented.

## 5.1 Results of the proposed ASSVCR technique

In order to evaluate the performance, the proposed ASSVCR technique is applied on several endoscopic images collected from Gastrolab [49] and Atlas [50]. The results are summarized below in four categories.

### *5.1.1 Category 1: Low-contrast color images*

In this case, the input image is first enhanced on the gray level and then color added. The chrominance values of the original input image are used for color reproduction. As a result, the output image has a similar color tone with strong contrast as shown in Fig. 5.1. It can be seen from the figure that the pit patterns, mucosa structures, defected polyps, tissue and vascular characteristics are better visible and highlighted in the output images, which can help the gastroenterologists in better diagnosis. The adaptive sigmoid function and uniform distribution provide focused visualization of pit patterns, mucosa structures and tissue characteristics; and space-variant color reproduction reproduce strong color contrast, which distinguishes the abnormalities in endoscopic images.

### *5.1.2 Category 2: Low-contrast grayscale images*

In this case, we show examples where low-contrast grayscale images are used (i.e., color information is not available for these images). The grayscale images are first enhanced and then

colorized using a theme image. The choice of the theme image is important as it may add color distortion if not properly chosen. Therefore, the theme images are selected from the same or similar physical location of the GI tract. The results of the enhanced images are shown in Fig. 5.2, along with the corresponding theme images.

### *5.1.3 Category 3: Raw NBI images*

In the next experiment, we applied the proposed ASSVCR technique on several NBI images (grayscale in nature) as shown in Fig. 5.3. The raw NBI images are enhanced first and then a color theme image is used to generate pseudo color. The theme images are chosen the same way as described before. It can be seen from the figure that the output images have a much better visibility of the mucosa structures, pit patterns and tissue characteristics compared to the grayscale NBI images.

### *5.1.4 Category 4: Image transmission in WCE*

The proposed color reproduction method is very useful in saving power consumption during transmission in WCE. Instead of transmitting all color images from the electronic capsule (which takes 24 bits per pixel per image), it can only transmit one color image at the beginning followed by a defined number of grayscale images (8 bits per pixel per image). Using the proposed ASSVCR technique, these grayscale images will be later colorized using the first color image at the receiver. Fig. 5.4 shows the result of such a case where the R, G and B components of frame 1 are transmitted first. Then only the luminance (Y) components of frame 2, 3, 4, and 5 are transmitted. At the receiver, these frames 2-5 are reconstructed using the proposed color reproduction method, taking frame 1 as the theme image. Later on, the color reconstructed images are compared with the original color video sequences. In the conventional case, the R, G, and B components of all frames are transmitted. For the given case, which includes five frames, it will require a total of 120 bits per pixel (i.e., 24 x 5). On the other hand, using the proposed

technique, it will require only 56 bits per pixel (i.e., 24+ 8 +8+8+8) will be required, which results in a saving of 53% during the transmission. More savings will be achieved using the number of grayscale frames is increased. The original color video frames are also shown in Fig. 5.4 for comparison. Here we see that the reconstructed output images have the same color as compared to the original color video frames with a power saving of 53%.

| No. | Input original image (color) | Enhanced grayscale image | Output enhanced color image |
|---|---|---|---|
| 1 |  (a) | 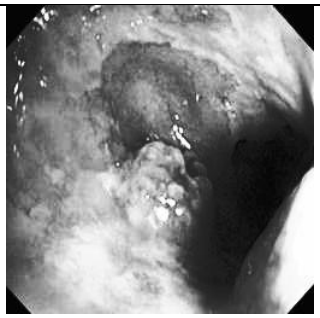 (b) | 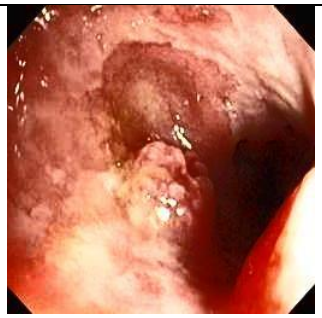 (c) |
| 2 | 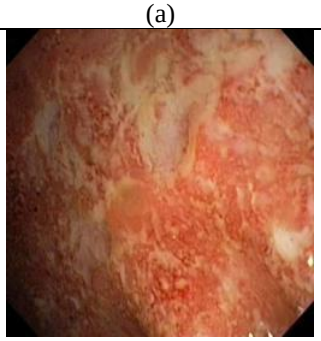 (d) | 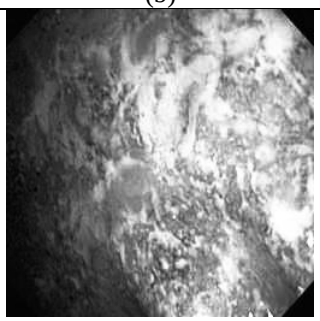 (e) | 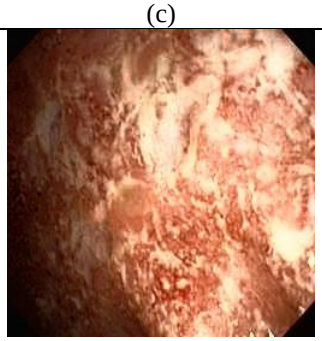 (f) |
| 3 | 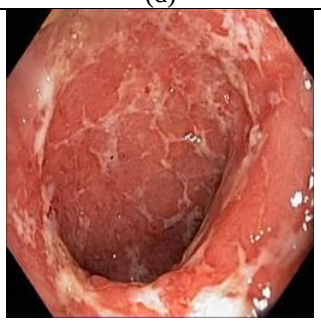 (g) | 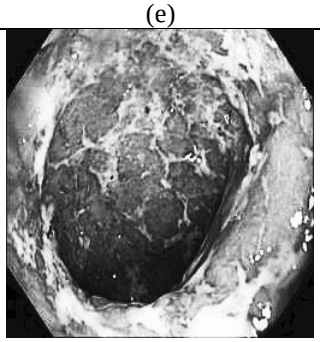 (h) |  (i) |
| 4 | 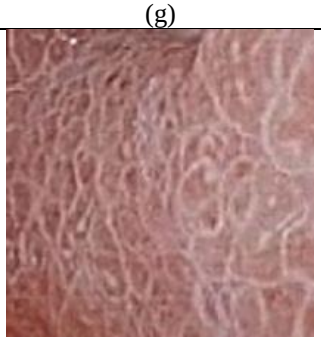 (j) | 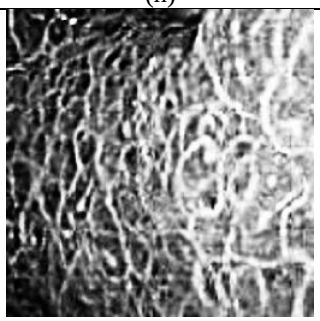 (k) | 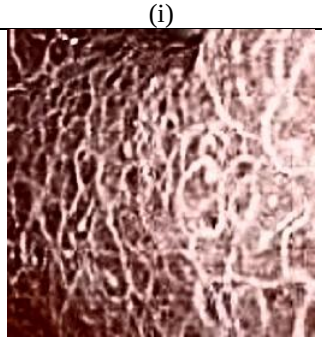 (l) |

Fig. 5.1 Category 1: Enhancement of colored WLI images (where input image is used as theme image) using the proposed ASSVCR technique

| No. | Input original image (grayscale) | Enhanced grayscale image | Theme image | Output enhanced color image |
|---|---|---|---|---|
| 1 | 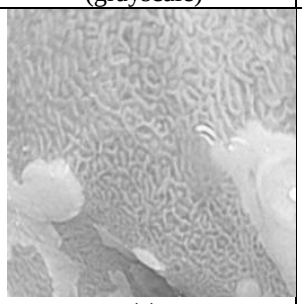 (a) | 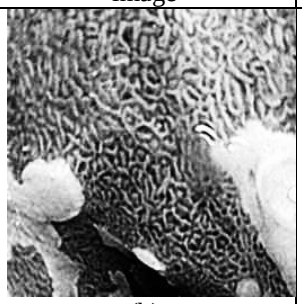 (b) |  (c) | 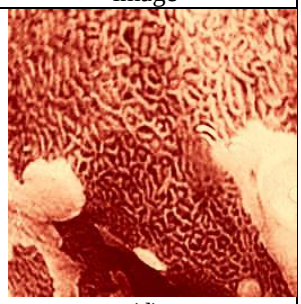 (d) |
| 2 | 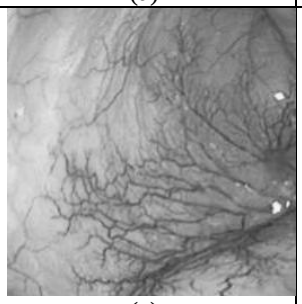 (e) | 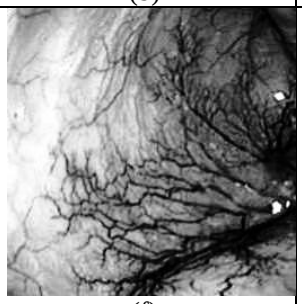 (f) | 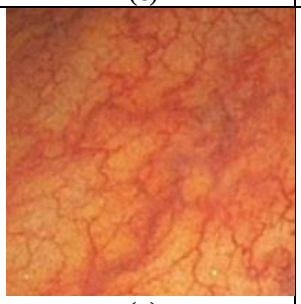 (g) | 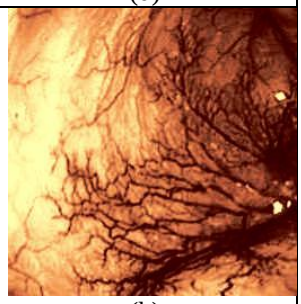 (h) |
| 3 | 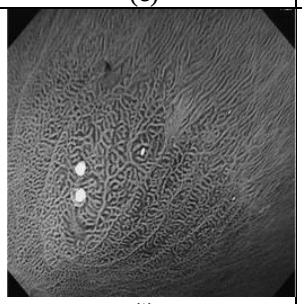 (i) | 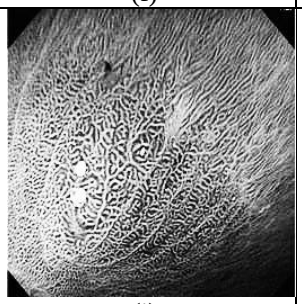 (j) | 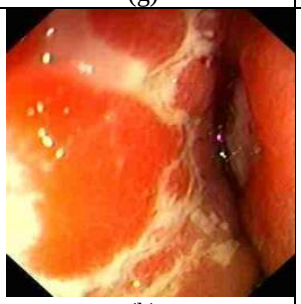 (k) | 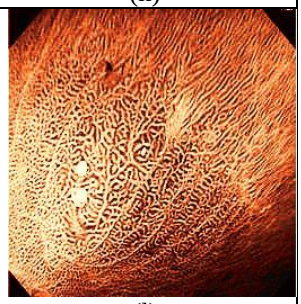 (l) |
| 4 | 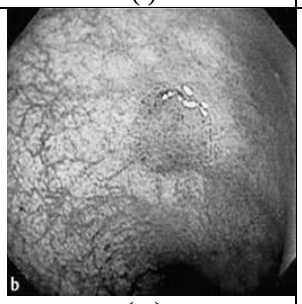 (m) | 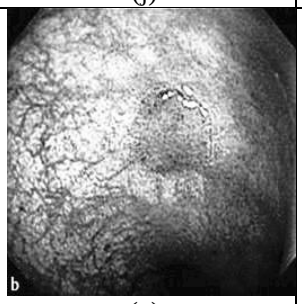 (n) | 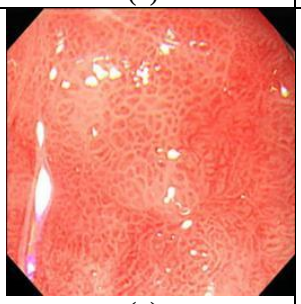 (o) | 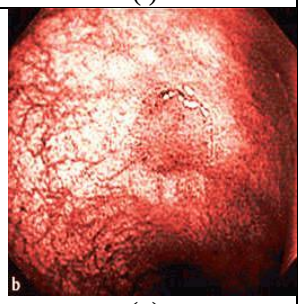 (p) |

Fig. 5.2 Category 2: Enhancement of grayscale WLI images (here, no original color image is available, so color image from similar location of the GI tract is used as theme image) using the proposed ASSVCR technique

| No. | Input RAW NBI image | Enhanced grayscale image | Theme image | Output enhanced color image |
|---|---|---|---|---|
| 1 | 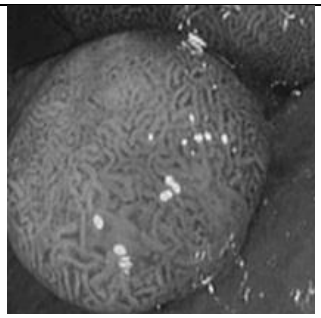 (a) | 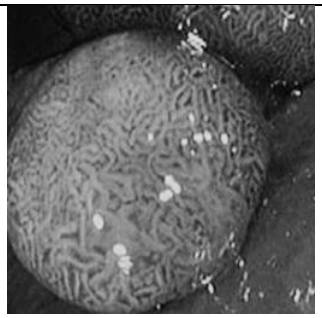 (b) |  (c) |  (d) |
| 2 | 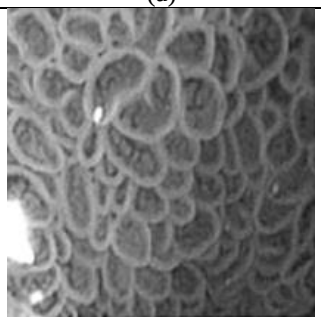 (e) | 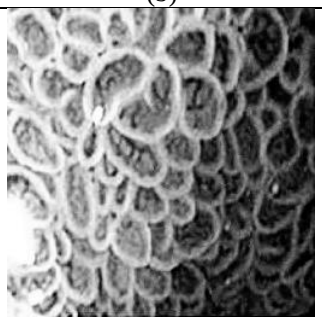 (f) | 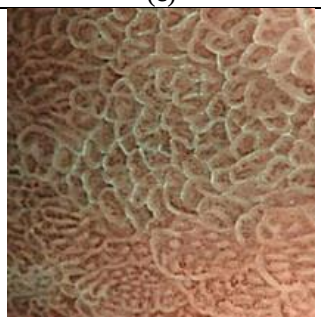 (g) | 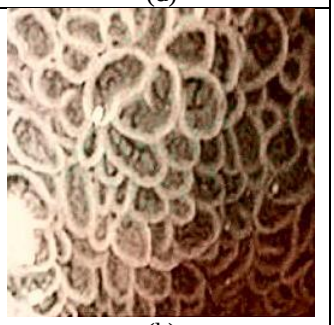 (h) |
| 3 | 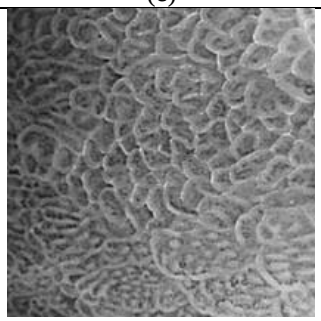 (i) | 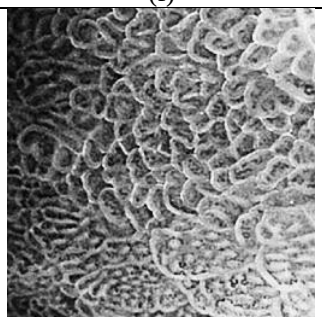 (j) |  (k) | 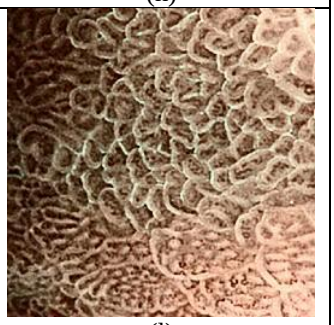 (l) |
| 4 | 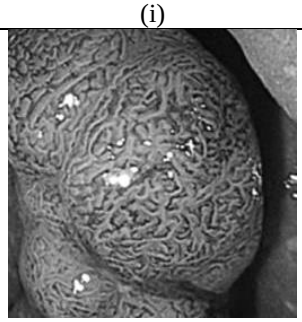 (m) | 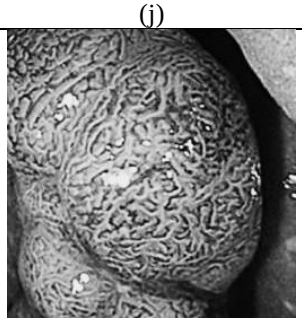 (n) |  (o) | 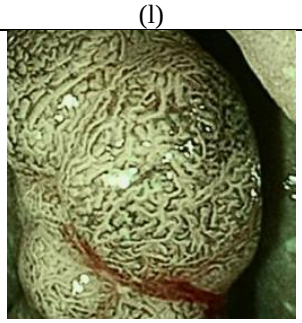 (p) |

Fig. 5.3 Category 3: Enhancement and color reproduction of grayscale NBI images using the proposed ASSVCR technique

| Frame no. | 1 | 2 | 3 | 4 | 5 |
|---|---|---|---|---|---|
| Original video frames |  |  | 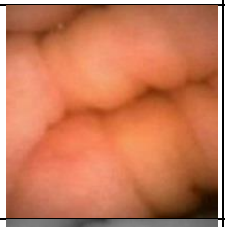 | 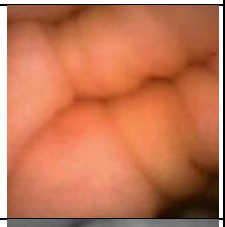 | 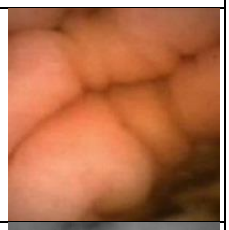 |
| Input images |  |  | 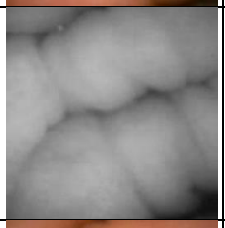 |  | 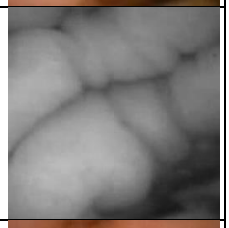 |
| Proposed color images (Frame #1 used as theme image) |  | 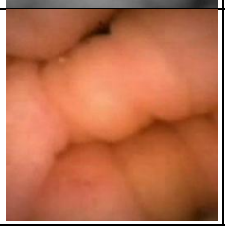 | 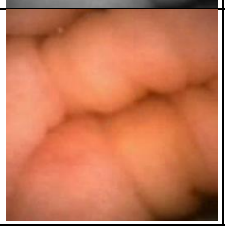 | 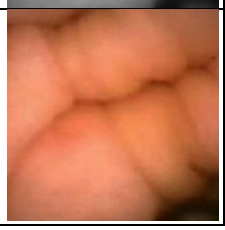 | 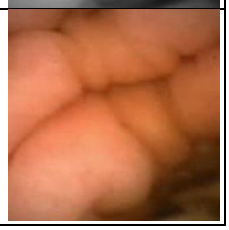 |

Fig. 5.4 Category 4: Reproduction of color frames from grayscale frame in WCE video; no enhancement was applied

## 5.2 Results of the proposed tri-scan technique

In order to evaluate the performance, the proposed tri-scan technique is applied on several endoscopic images collected from Gastrolab [49], Atlas [50] and FICE atlas [26] databases. The results are summarized below in four categories.

### *5.2.1 Category 1: Low contrast color images*

In this case, the tri-scan technique is applied on the different low contrast color endoscopic images. The results are presented in Fig. 5.5. Here, it is noticeable that the mucosa surfaces and tissue characteristics are more visible in the processed images compared to the original endoscopic image. It is because the proposed tri-scan technique use modified linear unsharp masking to sharpen the edges and borders of the images. It also enhances and highlights the micro-vessels of the superficial layers of the mucosa and sub-mucosa by using adaptive sigmoid function. The changes of the pattern and size of micro-vessels are also visible in the

processed images. In addition; the tri-scan creates light steel blue effect in the background, indian red effect on the surface and royal blue on the subtle mucosa layer by using 3-D uniform distribution, which distinguishes the pit patterns and abnormalities in the mucosa structures and layers.

### *5.2.2 Category 2: Comparison with NBI*

In this case, the proposed tri-scan is compared with NBI. The results are presented in Fig. 5.6. In Fig. 5.6 (1), it is noticeable that a Y-shape vein in the superficial layer of mucosa is only visible in the processed image, not in the original and NBI image. In Fig. 5.6 (2) and (4), the water shaded surfaces and pit patterns are clearly visible in the processed images. In Fig. 5.6 (3) and (5), the mucosa structures, size and pattern of micro-vessels in the processed images are more highlighted because of the light steel blue background effect.

### *5.2.3 Category 3: Comparison with FICE*

In this case, the tri-scan is compared with FICE. The results are presented in Fig. 5.7. In Fig. 5.7, it is noticeable that the mucosa structures, tissue and vascular characteristics, pattern of micro-vessels, superficial mucosa layer and pit patterns are better visible in processed images compared to the FICE images. In addition, it highlights the vascular characteristics better than the FICE, as shown in Fig. 5.7 image (1).

### *5.2.4 Category 4: Comparison with ME-NBI images*

In this case, the tri-scan is employed on magnified endoscopic (ME) NBI images for further enhancement. The results are presented in Fig.5.8. The mucosal structure, size and pattern of micro-vessels are better visible in processed images compare to the ME-NBI images.

| No. | Original image | Enhanced using tri-scan | No. | Original image | Enhanced using tri-scan |
|---|---|---|---|---|---|
| 1 |  | 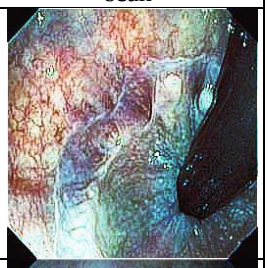 | 4 |  |  |
| 2 |  | 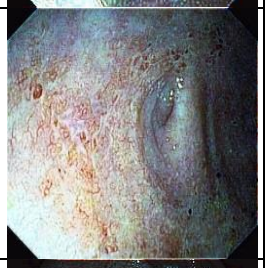 | 5 |  |  |
| 3 |  | 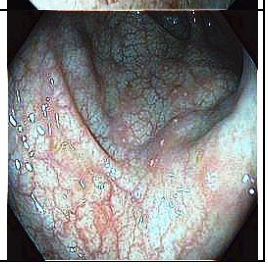 | 6 | 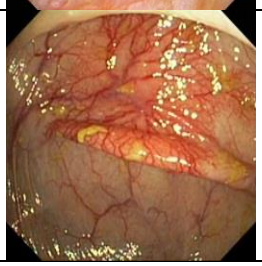 | 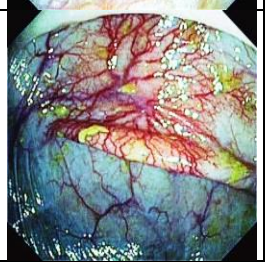 |

Fig. 5.5 Proposed tri-scan technique on different endoscopic images

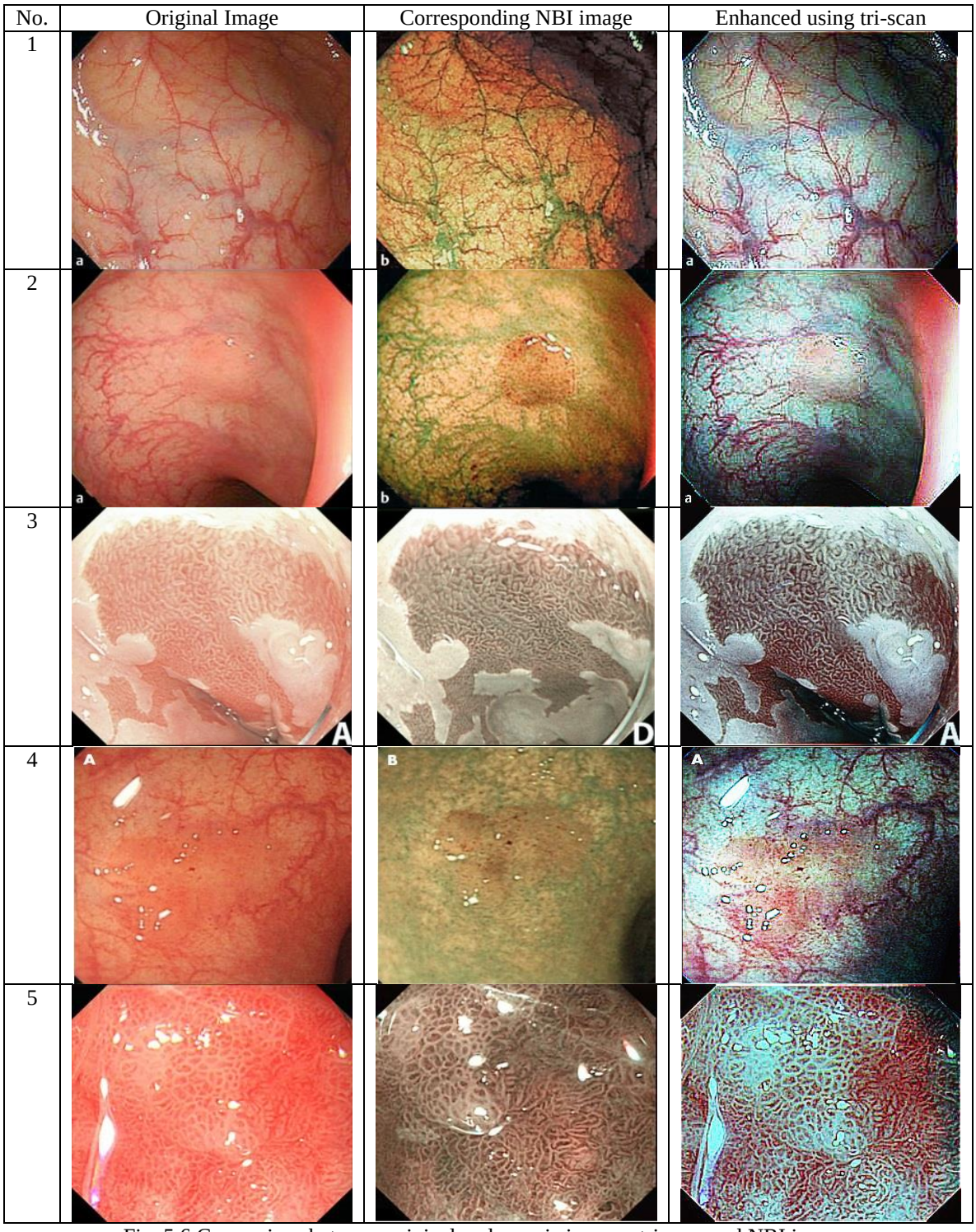


Fig. 5.6 Comparison between original endoscopic images, tri-scan and NBI images

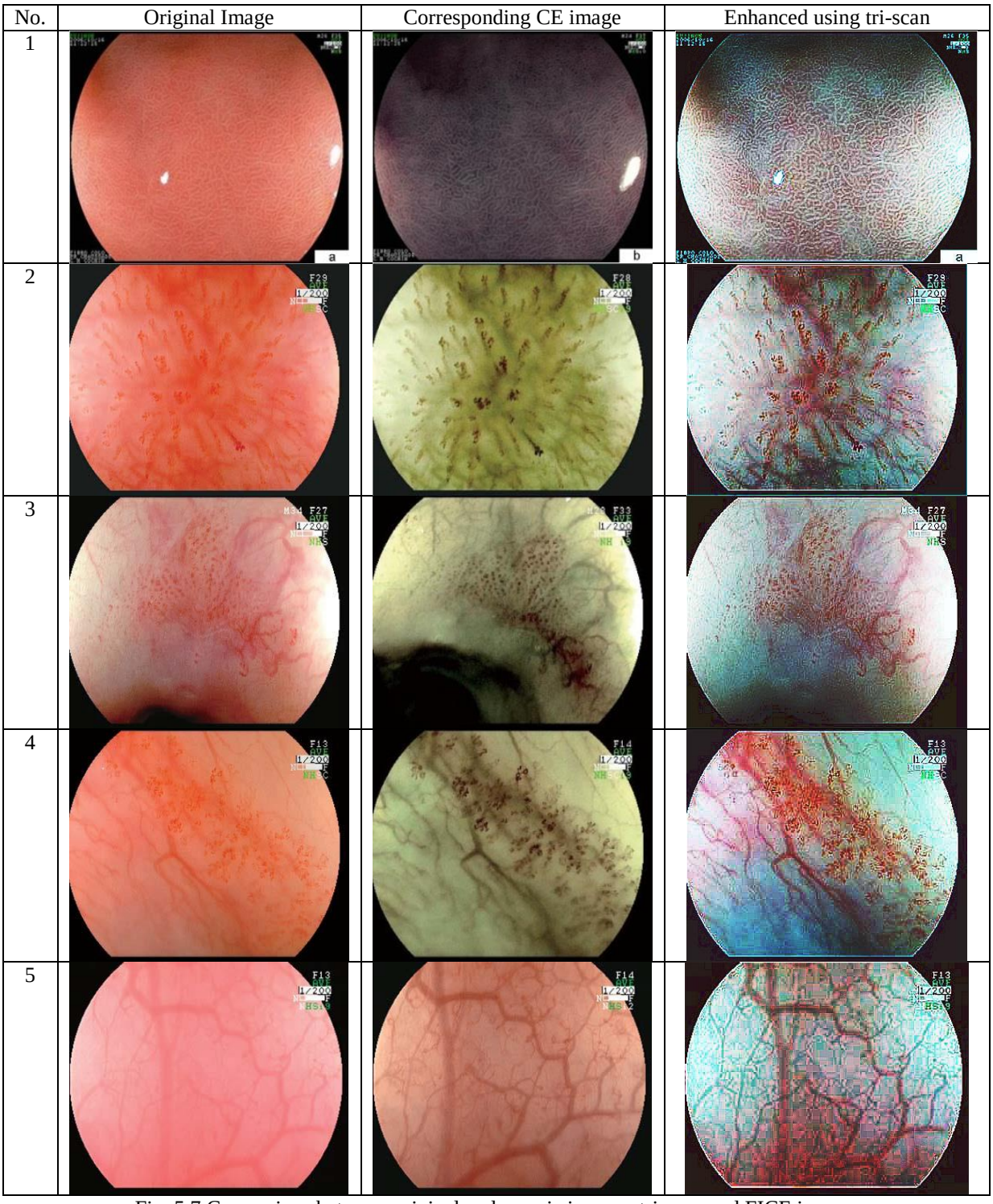


Fig. 5.7 Comparison between original endoscopic images, tri-scan and FICE images

| No. | Original ME-NBI image | Enhanced using tri-scan | No. | Original ME-NBI image | Enhanced using tri-scan |
|---|---|---|---|---|---|
| 1 | 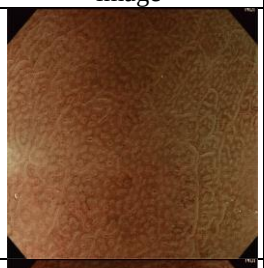 | 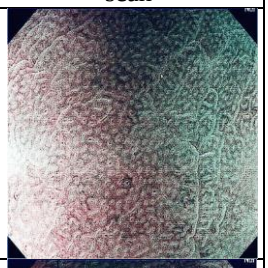 | 3 |  | 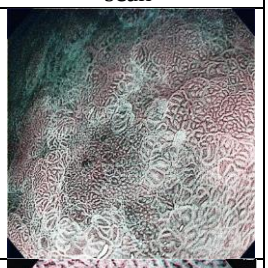 |
| 2 |  | 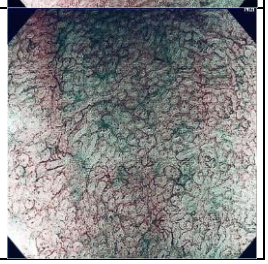 | 4 | 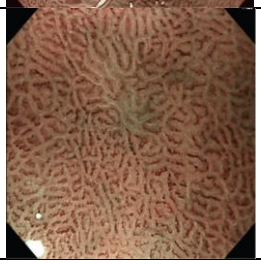 | 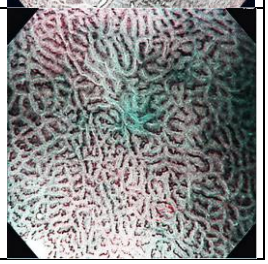 |

Fig. 5.8 Comparison between tri-scan and ME-NBI images

In summary, it can be concluded that both proposed techniques enhance and highlight features, such as tissue and vascular characteristics of mucosa structures and lesions, superficial layer of mucosal surface, size and pattern of micro-vessels, and abnormalities in GI tract which is not clearly visible in the original images. The proposed ASSVCR technique is more appropriate to enhance the original image with strong color contrast or grayscale image. Moreover, its advantages of color reproduction can be utilized to save more power in WCE transmission. The tri-scan technique is more appropriate for those color endoscopic images where gastroenterologists want to see more subtle features and abnormalities in pseudo color background same as NBI and FICE techniques.

## 5.3 Comparative analysis between the ASSVCR and tri-scan techniques

Both techniques can greatly enhance the subtle features of endoscopic images, but their approaches toward enhancement are different. A comparative analysis of the two techniques is briefly presented in the following table:

**Table 5.1 A comparative analysis of two proposed techniques**

| | Proposed ASSVCR | Proposed tri-scan |
|---|---|---|
| Input image | Can be a color image or grayscale image | Only the color image can be used |
| Theme image | If the input image is a grayscale image then a theme image is required for the color reproduction. Additionally, the theme image must be selected from the same or similar physical location of GI tract | No theme image is required |
| Image enhancement | Applied on gray level of image | Applied on each color plane of a RGB image |
| Enhancement type | Only the global approach is employed | Both local and global approaches are employed |
| Color reproduction | Used for retrieving the original color with strong contrast | No color reproduction is required |
| Color type of Output image | Original color with strong contrast | Pseudo color |
| Feature extracted | Capable of enhancing and highlighting mucosa surfaces and structures, tissue and vascular characteristics, pit patterns and abnormal growths; however, it cannot highlight superficial layer of mucosa, and size and pattern of micro-vessels of endoscopic images | Capable of enhancing and highlighting all the six features of endoscopic images |

| | Proposed ASSVCR | Proposed tri-scan |
|---|---|---|
| Feature highlighted | Features are highlighted in original color | Features are highlighted in pseudo color |
| Image type | Applicable for color endoscopic images, grayscale images, grayscale NBI and AFI images | Applicable for only color endoscopic and ME-NBI images |
| Time complexity | Medium | Low |
| Power consumption | Useful in saving power consumption during the transmission in WCE | No benefit in the transmission end |

From the above table, it is concluded that the functionalities between the two techniques are different. The ASSVCR technique is more appropriate for the gastroenterologists who require the enhancement of endoscopic image features without changing the original color tone, or when only grayscale endoscopic images are available. On the other hand, the tri-scan is more suitable for enhancing and distinguishing the features by adding pseudo color.

# Chapter 6: Performance analysis

This chapter presents the performance analysis of the two proposed techniques. Here, both of the techniques are evaluated objectively using several performance metrics, such as focus value, statistic of visual representation, measurement of uniform distribution, color similarity test, color enhancement factor (CEF) and time complexity, with other related works. First, the ASSVCR technique is evaluated with other related digital imaging techniques because it performs enhancement at the gray level and reproduce original color, which more relates with digital imaging. The related digital imaging techniques are: AHE, CLAHE, BPDFHE and HBF. Finally, the tri-scan technology is evaluated with NBI and FICE because the color enhancement reproduces pseudo color to distinguish abnormalities and other features, which is similar to the techniques of NBI and FICE. Finally, a comparative analysis is presented between the ASSVCR and tri-scan techniques. The results and analysis are presented below.

## 6.1 Performance analysis of the proposed ASSVCR technique

In following section, the performance of ASSVCR is evaluated using focus value, statistic of visual representation, measurement of uniform distribution, color similarity test, color enhancement factor (CEF) and time complexity with other related digital imaging techniques. The results are discussed below:

### *6.1.1 Focus value*

In the proposed ASSVCR technique, image enhancement is performed by adaptive sigmoid function and uniform distribution of sigmoid pixels. As a result, the overall information of sharp counters and contrast is increased. These changes of an image are evaluated using focus value [51]. Focus value is a mathematical representation of the ratio of AC and DC energy of a

Discrete Cosine Transform (DCT) image [52]. Let $E_{AC}$ and $E_{DC}$ be the energy of AC and DC components of the DCT image as given below:

$$E_{DC} = (F_{DC}(u,v))^2 \tag{6.1}$$

$$E_{AC} = \sum_{u=1}^{n} \sum_{v=1}^{m} (F_{AC}(u,v) - \overline{F_{AC}(u,v)})^2 \tag{6.2}$$

Here, $u$ and $v$ represent the row and column of the DCT images, $F_{DC}$ is the DC part and $F_{AC}$ is the AC part of DCT image. The resultant of the ratio of $E_{AC}$ and $E_{DC}$ is the focus value $F_S$ as given by Equation (6.3):

$$F_S = \frac{E_{AC}}{E_{DC}} \tag{6.3}$$

If the overall information of sharp counters, crisp edges and contrast of enhanced image is higher than the original image, then its $F_S$ will be higher than the original image and vice versa. Here, the ASSVCR technique is compared in terms of focus value using sixty sample images with other related techniques like AHE [28], CLAHE [29], HBF [30] and BPDFHE [31]. The results are presented in Table 6.1

**Table 6.1 Comparisons of focus value with other related works**

| Image no. | Focus value | | | | | |
|---|---|---|---|---|---|---|
| | Original | AHE [28] | CLAHE [29] | HBF [30] | BPDFHE [31] | ASSVCR |
| 1 | 15.64 | 17.50 | 22.96 | 22.86 | 22.04 | 42.10 |
| 2 | 12.52 | 16.75 | 20.14 | 19.33 | 17.11 | 42.52 |
| 3 | 18.01 | 19.20 | 23.18 | 22.40 | 22.00 | 41.57 |
| 4 | 13.66 | 18.85 | 22.01 | 20.97 | 20.51 | 42.00 |
| Avg. of 60 endoscopic image | 13.77 | 19.08 | 21.11 | 20.49 | 19.49 | 41.17 |

It is noticeable that the focus values of the proposed ASSVCR are relatively higher when compared with the other techniques.

### *6.1.2 Statistic of visual representation*

Next, the statistic of visual representation [53] is used to evaluate the proposed ASSVCR technique. It measures the contrast and intensity distortion between two processed images. Equations (16) and (17) represent the statistic visual representation.

$$C = \frac{\sigma_{out} - \sigma_{in}}{\sigma_{in}} \tag{6.4}$$

$$L = \frac{L_{out} - L_{in}}{L_{in}} \tag{6.5}$$

Where, $\sigma_{out}$ and $L_{out}$ are the variance and mean of enhanced image; $\sigma_{in}$ and $L_{in}$ are the variance and mean of original image, respectively. Here, C defines the percentage increment or decrement of contrast level and $L$ defines the percentage increment or decrement in intensity level. In our experiment, sixty grayscale endoscopic images are used. The results are presented in Table 6.2. It is noticeable that the $C$ and $L$ of the first image, using the ASSVCR technique are 1.0636 and 0.0716, which means the contrast and intensity level of the processed image by ASSVCR are 103.6 and 7.16 times higher, respectively, than the original image. Here, the negative sign denotes the decrement. It is noticeable that the proposed ASSVCR technique's contrast level and intensity level are higher compared to the other digital imaging techniques.

**Table 6.2 Comparisons of statistic of visual representation with other related works**

| Image no. | Contrast measurement | | | | | Intensity measurement | | | | |
|---|---|---|---|---|---|---|---|---|---|---|
| | AHE [28] | CLAHE [29] | HBF [30] | BPDFHE [31] | ASSVCR | AHE [28] | CLAHE [29] | HBF [30] | BPDFHE [31] | ASSVCR |
| 1 | 0.3373 | 0.4735 | 0.4285 | 0.2025 | 1.0636 | -0.1781 | 0.0598 | 0.0254 | 0.0065 | 0.0716 |
| 2 | 0.2767 | 0.6352 | 0.2395 | 0.3608 | 2.4684 | -0.0312 | 0.1207 | 0.0095 | 0.0092 | 0.2526 |
| 3 | 0.1205 | 0.2935 | 0.2395 | 0.1192 | 1.12294 | -0.1122 | 0.0410 | 0.0095 | -0.0012 | 0.1322 |
| 4 | 0.3401 | 1.1598 | 0.8235 | 0.7206 | 2.0349 | -0.1186 | -0.0291 | 0.0134 | -0.0100 | 0.0218 |
| Avg. of 60 endoscopic images | 0.2554 | 0.6411 | 0.4149 | 0.3371 | 1.6147 | -0.1203 | 0.0381 | 0.0197 | 0.0174 | 0.1748 |

### *6.1.3 Measurement of uniform distribution*

Here, the uniform distribution of R, G and B planes of processed images using ASSVCR technique is calculated [54] [55]. The higher uniform distribution value denotes better color enhancement. The uniform distribution of $n$ distributed signals is defined by,

$$H(x_1, x_2, ..., x_n) = -\sum_{x_1}\sum_{x_2}...\sum_{x_n} P(x_1, x_2, .., x_n) \times \log_2 P(x_1, x_2, .., x_n) \qquad (6.6)$$

First, the advantage of using the ASSVCR is shown in Fig. 6.1. Here, in image (a), we used the ASSVCR on the luminance plane and left the chrominance planes unchanged. In image (b), we applied the ASSVCR on luminance and color reproduction on the chrominance planes. From both images, it is noticeable that the image in (a) without color reproduction does not preserve brightness and shows an imbalanced saturation level. Contrarily, the image in (b) with color reproduction has a balanced saturation and preserves the overall brightness. It happens because *YCbCr* is a non-uniform and non-orthogonal color space. That is why we need to manipulate both luminance and chrominance in such a way that the correlation does not break, in order to preserve the brightness along with the color saturation level.

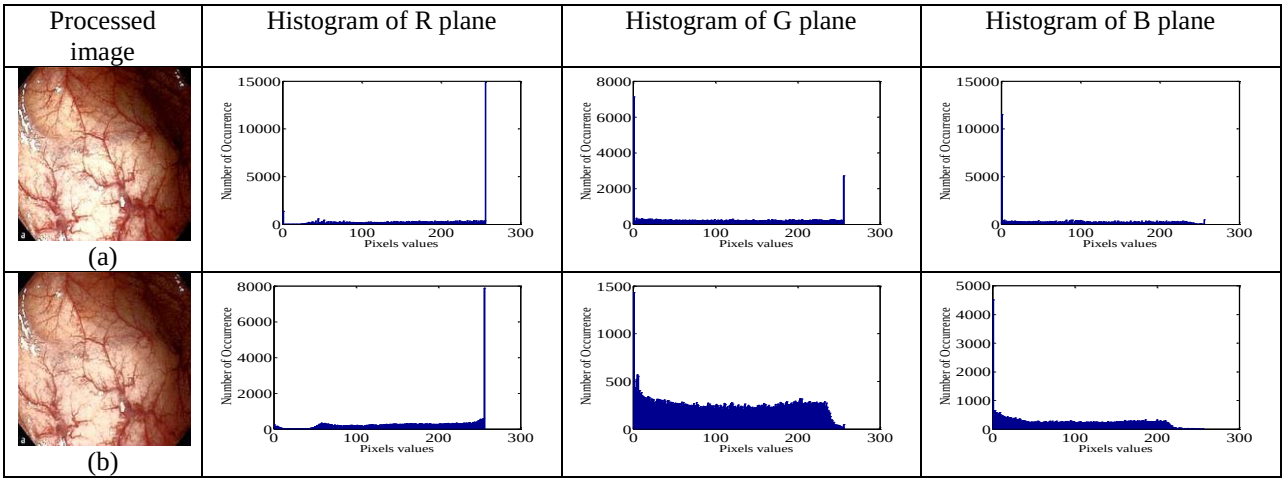


Fig. 6.1 Histogram of R, G and B plane in terms of uniform distribution (a) without and (b) with color reproduction

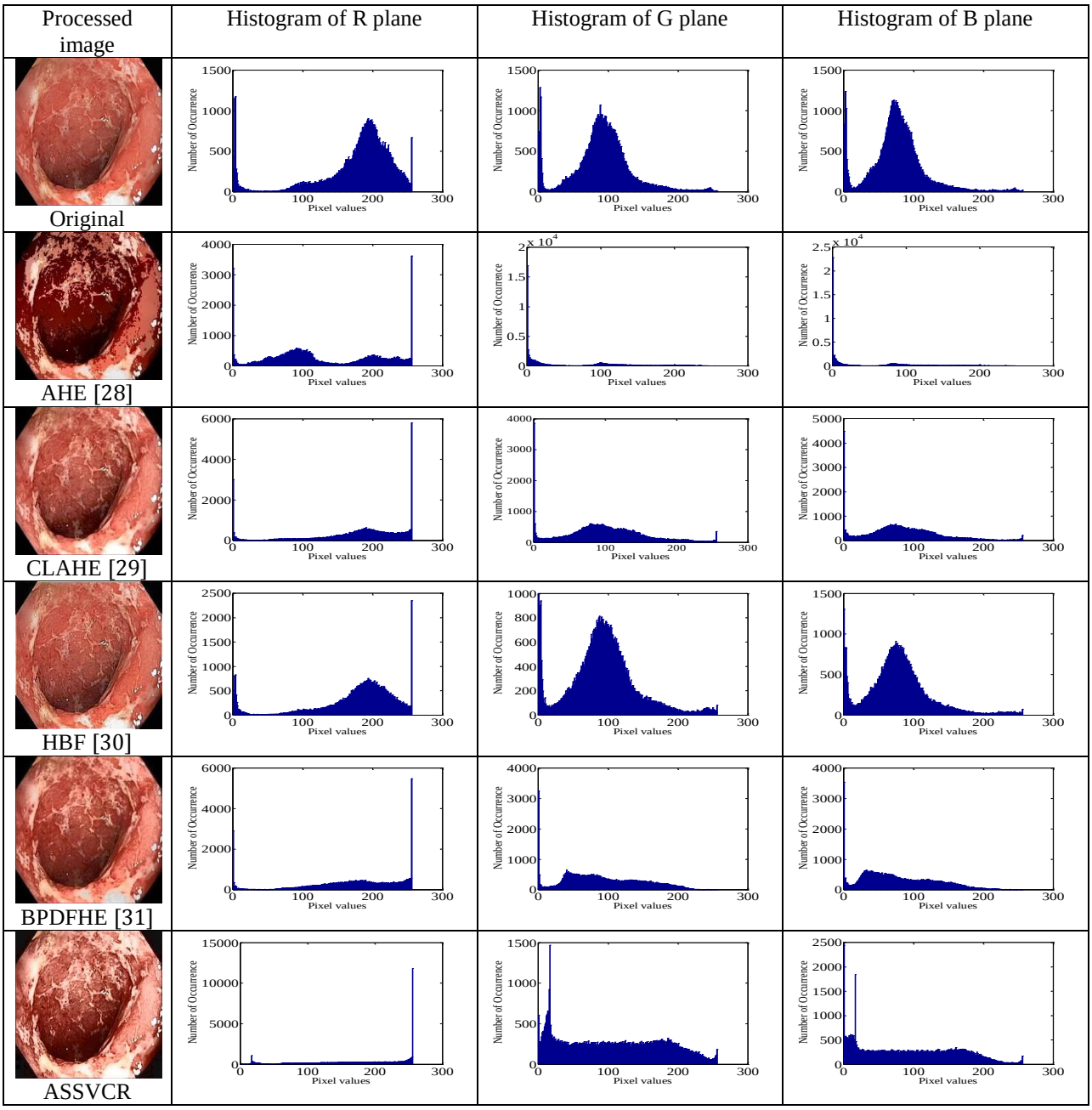


Fig. 6.2 Comparison of the histogram of R, G and B planes in terms of uniform distribution

Additionally, the ASSVCR technique achieves a higher uniform distribution value, which means that it produces a more uniform histogram. The entropy value of image (b) is 7.6237, which is higher than that of image (a), which is at 7.4961. Fig. 6.2 shows the performance comparison with other digital imaging techniques. It shows that the ASSVCR produces images

with enhanced and highlighted mucosa structures and tissue characteristics. The results are also summarized in Table 6.3.

**Table 6.3 Comparisons of the uniform distribution based on entropy with other related works**

| Image no. | Measurement of entropy | | | | | |
|---|---|---|---|---|---|---|
| | Original | AHE [28] | CLAHE [29] | HBF [30] | BPDFHE [31] | ASSVCR |
| 1 | 7.25 | 6.68 | 7.38 | 7.33 | 7.41 | 7.46 |
| 2 | 7.21 | 6.47 | 7.48 | 7.33 | 7.44 | 7.57 |
| 3 | 7.11 | 6.38 | 7.34 | 7.31 | 7.38 | 7.51 |
| 4 | 6.52 | 4.87 | 7.11 | 6.77 | 7.51 | 7.70 |
| Avg. of 60 endoscopic images | 7.41 | 7.01 | 7.68 | 7.31 | 7.75 | 7.91 |

### *6.1.4 Color similarity test*

To validate the results statistically, the color similarity between the original and color reproduced images are evaluated using CIE94 delta-E color difference [56], mean structure similarity index (MSSIM) [57] and structure and hue similarity (SHSIM) [58]. The purpose is to show that proposed ASSVCR technique does not add any additional color. CIE94 is used to measure the color differences between the processed images by ASSVCR and original image in LAB color space. In CIE94, $\Delta E_{94}^{*} \approx 2.3$ indicates, which color difference is the lowest when comparing the two images. MSSIM is used to measure color similarity in the chrominance planes in YCbCr color space. SHSIM is used to measure the hue and structure similarity between the processed and original image in HSV color space. Here, sixty trial images are used to evaluate the color similarity index. The results are compared with other color reproduction methods, and presented in Table 6.4. It can be determined that the average MSSIM and SHSIM indices are higher than others in our scheme with a color difference $\Delta E_{94}^{*}$ close to 2.3. All of these values indicate that the color tone reproduced by the proposed ASSVCR technique is close to the original image.

**Table 6.4 Color similarity assessment**

| Similarity between two color images | | $\Delta E^*_{94}$ | MSSIM | SHSIM |
|---|---|---|---|---|
| Image 1 | Image 2 | | | |
| Original image | ASSVCR | 2.97 | 0.9851 | 0.9992 |
| | Welsh [35] | 4.1 | 0.8605 | 0.8578 |
| | Valeriy [38] | 0.6 | 0.8714 | 0.8001 |
| | Imtiaz [40] [39] | 3.01 | 0.9567 | 0.9942 |

### *6.1.5 Color enhancement factor (CEF)*

The proposed ASSVCR technique is also evaluated in terms of color enhancement. Here, a no-reference performance metric called colorfulness matric (CM) [59] is used. The CM measurement is based on the mean and standard deviations of two axis opponent color representation with, $\alpha = R - G$ and $\beta = \frac{1}{2}(R+G) - B$. The metric is defined as:

$$CM = \sqrt{\sigma_\alpha^2 + \sigma_\beta^2} + 0.3\sqrt{\mu_\alpha^2 + \mu_\beta^2} \tag{6.7}$$

Where, $\sigma_\alpha$ and $\sigma_\beta$ are standard deviations of $\alpha$ and $\beta$, respectively. Similarly, $\mu_\alpha$ and $\mu_\beta$ are their means. However, in our comparison, the ratio of CMs between the enhanced and original image is employed for observing the color enhancement factor (CEF). If $CEF < 1$, than the original image is better when compared to the enhanced image in terms of color image enhancement and vice versa. $CEF = 1$ indicates that there is no difference between the enhanced and original image in terms of color enhancement. The results are presented in Table 6.5 and Table 6.6. Here it is noticeable that the CEF values of ASSVCR are highest when compared to other enhancement methods as well as other related color reproduction methods, which indicates that our scheme performs better in terms of color enhancement. Fig. 6.3 shows some reconstructed images.

**Table 6.5 Comparisons of CEF indices with other enhancement works**

| Image no. | AHE [28] | CLAHE [29] | HBF [30] | BPDFHE [31] | ASSVCR |
|---|---|---|---|---|---|
| 1 | 0.9620 | 1.1197 | 1.0355 | 1.0149 | 1.7329 |
| 2 | 0.9623 | 1.0989 | 1.0077 | 1.0037 | 1.8897 |
| 3 | 0.9446 | 1.1716 | 1.0751 | 1.0547 | 1.8812 |
| 4 | 0.9946 | 1.2009 | 1.1913 | 1.1003 | 1.7443 |
| Avg. of 60 endoscopic images | 0.9661 | 1.1574 | 1.0614 | 1.0411 | 1.7477 |

**Table 6.6 Comparisons of CEF indices with other color reproduction works**

| Image no. | Imtiaz [40] [39] | Welsh [35] | Valeriy [38] | ASSVCR |
|---|---|---|---|---|
| 1 | 1.1059 | 0.5987 | 0.5118 | 1.7784 |
| 2 | 1.0991 | 0.7481 | 0.5997 | 1.6599 |
| 3 | 1.1007 | 0.6187 | 0.6001 | 1.8413 |
| 4 | 1.1972 | 0.5249 | 0.4991 | 1.7749 |
| Avg. of 60 endoscopic images | 1.1391 | 0.5149 | 0.4977 | 1.5621 |

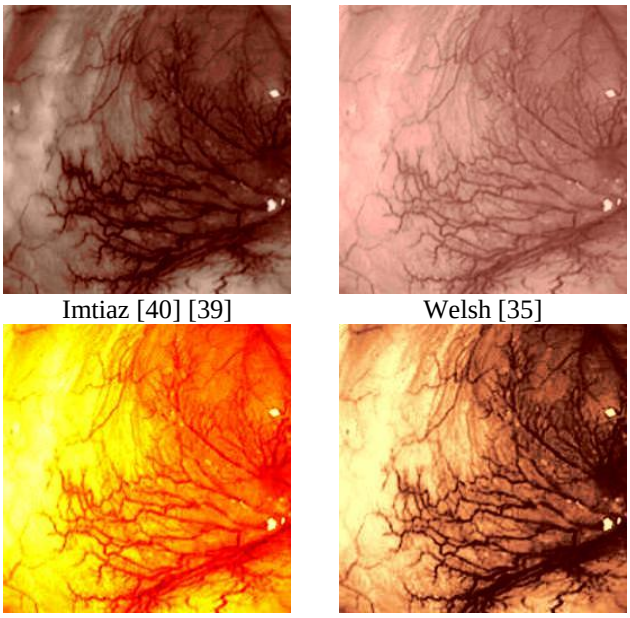

Imtiaz [40] [39] Welsh [35]

Valeriy [38] ASSVCR

Fig. 6.3 Enhanced color images using different color reproduction algorithms

### *6.1.6 Time complexity*

The time that is required to generate an enhanced color image for different image sizes using the ASSVCR technique and other related works [35] [38] [39] [40] are shown in Table 6.7. The experiment was conducted on a PC having Intel (R) Pentium(R) dual CPU @ 2.00GHz and 6 GB of RAM. Here, it is noticeable that the proposed ASSVCR technique is faster including

both image enhancement and color reproduction. For an image of *n* pixels, the ASSVCR technique has linear computational time complexity, *O(n)*. The average simulation time of the ASSVCR technique for 256×256 images is approximately 20 seconds and for 512×512 images, is approximately 80 seconds. The work in [35] [39] [40] have significantly higher execution time when compared with the ASSVCR technique. Although the execution time of [38] is lower than the ASSVCR, the quality of the color reproduction is more flat and dull, as shown in Fig. 6.3.

**Table 6.7 Comparison of simulation speed between the proposed ASSVCR technique and other related works**

| Methodology | Image size | Step 1 | Step 2 | Total time (sec) |
|---|---|---|---|---|
| | | Enhancement time (sec.) | Color reproduction time (sec.) | |
| ASSVCR | 256x256 | 1.909 | 20.614 | 22.523 |
| | 512x256 | 2.597 | 40.119 | 42.716 |
| | 512x512 | 3.182 | 81.779 | 84.961 |
| [40] [39] | 256x256 | 0.39 | 28.255 | 28.645 |
| | 512x256 | 1.519 | 72.956 | 74.475 |
| | 512x512 | 1.525 | 113.31 | 114.835 |
| [35] | 256x256 | - | 64.461 | 64.461 |
| | 512x256 | - | 117.921 | 117.921 |
| | 512x512 | - | 232.146 | 235.149 |
| [38] | 256x256 | - | 0.19 | 0.19 |
| | 512x256 | - | 0.81 | 0.81 |
| | 512x512 | - | 0.47 | 0.47 |

## 6.2 Performance analysis of the proposed tri-scan

In the following section, the performance of the proposed tri-scan is evaluated using focus value, statistic of visual representation, and color enhancement factor (CEF) with other related techniques like NBI [18] and FICE [26]. The results are discussed below:

### *6.2.1 Focus value*

In the tri-scan technique, the enhancement is employed in each plane in three different stages for highlighting mucosa structures and tissue characteristics. Eventually, the overall

information of sharp counters, edges and contrast are increased. These changes of an image are evaluated using focus value [51] [52] using (6.3). Here, the tri-scan technique is compared in terms of focus value using sixty sample images with other techniques; NBI [18] and FICE [26].

**Table 6.8 Comparisons of focus value with NBI**

| Image no. | Focus value | | |
|---|---|---|---|
| | Original | NBI [18] | Tri-scan |
| 1 | 11.33 | 25.67 | 39.68 |
| 2 | 13.12 | 27.29 | 40.15 |
| 3 | 8.74 | 16.17 | 30.67 |
| 4 | 5.29 | 9.25 | 40.53 |
| 5 | 9.47 | 14.28 | 29.13 |
| Avg. of 60 endoscopic image | 17.63 | 20.71 | 38.78 |

**Table 6.9 Comparisons of focus value with FICE**

| Image no. | Focus value | | |
|---|---|---|---|
| | Original | FICE [26] | Tri-scan |
| 1 | 26.84 | 22.36 | 39.18 |
| 2 | 26.68 | 35.06 | 43.89 |
| 3 | 34.12 | 55.81 | 66.98 |
| 4 | 33.49 | 38.06 | 46.01 |
| 5 | 33.29 | 37.47 | 41.28 |
| Avg. of 60 endoscopic image | 28.71 | 36.49 | 45.11 |

Here, it is noticeable that the focus values of tri-scan are relatively higher compared to the other methods.

### *6.2.2 Statistic of visual representation*

Next, the proposed tri-scan technique is compared in terms of statistic of visual representation [53] using (6.6). The results are also compared with other related works. They are presented in Table 6.10 and Table 6.11. It is noticeable that the $C$ and $L$ of the first image are 1.7597 and 0.0699, which means the contrast and intensity level of processed images by the tri-scan are 175.9 and 6.99 times higher than the original image respectively. Here, the negative sign denotes the decrement.

**Table 6.10 Comparisons of statistic of visual representation between NBI and tri-scan**

| Image no. | Contrast measurement | | Intensity measurement | |
|---|---|---|---|---|
| | NBI [18] | Tri-scan | NBI [18] | Tri-scan |
| 1 | 1.2480 | 1.7597 | -0.0169 | 0.0699 |
| 2 | 1.2076 | 1.8823 | -0.0782 | 0.0516 |
| 3 | 1.2163 | 1.6856 | -0.0931 | 0.3054 |
| 4 | 2.0255 | 2.8647 | -0.0122 | 0.0092 |
| 5 | 1.1697 | 1.7294 | -0.2234 | 0.1649 |
| Avg. of 60 endoscopic image | 1.4253 | 1.9381 | -0.0549 | 0.0901 |

**Table 6.11 Comparisons of statistic of visual representation between FICE and tri-scan**

| Image no. | Contrast measurement | | Intensity measurement | |
|---|---|---|---|---|
| | FICE [26] | Tri-scan | FICE [26] | Tri-scan |
| 1 | 0.9876 | 1.5460 | -0.4818 | 0.0680 |
| 2 | 1.0422 | 1.6565 | -0.0511 | 0.0217 |
| 3 | 0.9411 | 1.1160 | -0.1985 | 0.0105 |
| 4 | 0.7020 | 1.4578 | -0.0933 | 0.0161 |
| 5 | 0.6216 | 1.5192 | -0.1974 | 0.1428 |
| Avg. of 60 endoscopic image | 0.7947 | 1.5016 | -0.1958 | 0.0819 |

It can be concluded from the above tables that the tri-scan technique's contrast level and intensity level are higher compare to the level of other methods.

### *6.2.3 Color enhancement factor (CEF)*

Finally, the tri-scan is evaluated in terms of color enhancement. Here, a no-reference performance metric called colorfulness matric (CM) [59] is used (6.7). However, in our comparison, we have used the ratio of CMs between the enhanced and original image for observing the color enhancement factor (CEF). The tri-scan is compared in terms of CEF using sixty sample images with other techniques like NBI [18] and FICE [26]. The results are presented in Table 6.12 and Table 6.13.

**Table 6.12 Comparisons of CEF with NBI**

| Image no. | CEF | |
|---|---|---|
| | NBI [18] | Tri-scan |
| 1 | 1.1998 | 1.5478 |
| 2 | 1.0453 | 1.4633 |
| 3 | 1.0072 | 1.7076 |
| 4 | 1.0584 | 1.5716 |
| 5 | 1.2725 | 1.6453 |
| Avg. of 60 endoscopic image | 1.2214 | 1.5119 |

**Table 6.13 Comparisons of CEF with FICE**

| Image no. | CEF | |
|---|---|---|
| | FICE [26] | Tri-scan |
| 1 | 1.1733 | 1.4716 |
| 2 | 1.3464 | 1.4788 |
| 3 | 1.4325 | 1.5010 |
| 4 | 1.3788 | 1.7222 |
| 5 | 1.3747 | 1.7244 |
| Avg. of 60 endoscopic image | 1.2711 | 1.5549 |

Here, it is noticeable that CEF values of the tri-scan are highest when compared to other techniques, which indicates that our scheme performs better in terms of color enhancement.

## 6.3 Performance analysis of the proposed ASSVCR and tri-scan techniques

Here, the performance of the two proposed techniques is evaluated. In the previous chapter, it has been shown that proposed ASSVCR and tri-scan techniques have different enhancement approaches. However, it is possible to evaluate which technique has better enhancement in terms of contrast levels, intensity levels and sharpness using the focus value and statistic of visual representation. The ASSVCR and tri-scan are also compared based on time complexity. The results are briefly discussed below.

### *6.3.1 Focus value*

Here, focus value [51] is used to evaluate which proposed technique is more suitable for increasing contrast and sharpening the edges and counters. The results are presented in Table

6.14. Here, it can be observed that tri-scan is better when compared to the ASSVCR technique, in respect to contrast increments, and sharpening the edges and counters.

**Table 6.14 Comparisons of focus value between two proposed techniques**

| Image no. | Focus value | |
|---|---|---|
| | ASSVCR | Tri-scan |
| 1 | 14.57 | 40.11 |
| 2 | 13.74 | 37.83 |
| 3 | 19.77 | 35.54 |
| 4 | 14.81 | 29.01 |
| 5 | 16.01 | 41.93 |
| Avg. of 20 endoscopic images | 17.09 | 36.88 |

### *6.3.2 Statistic of visual representation*

The statistic of visual representation [53] is used to measure the contrast and intensity of the proposed techniques. Here, it will measure the increment or decrement of contrasts and intensities between the original image and the processed image using both techniques. The results are presented in Table 6.15.

**Table 6.15 Comparisons of statistic of visual representation between two proposed techniques**

| Image no. | Statistic of visual representation | | | |
|---|---|---|---|---|
| | ASSVCR | | Tri-scan | |
| | Contrast | Intensity | Contrast | Intensity |
| 1 | 1.1246 | 0.0021 | 1.9915 | 0.1478 |
| 2 | 1.0047 | 0.0233 | 1.5329 | 0.5271 |
| 3 | 1.1091 | 0.1091 | 1.7451 | 0.4051 |
| 4 | 1.2237 | 0.0074 | 2.0315 | 0.1015 |
| 5 | 1.3916 | 0.2457 | 1.9177 | 0.7516 |
| Avg. of 20 endoscopic images | 1.1604 | 0.0875 | 1.8749 | 0.3741 |

Here, it can be observed that tri-scan technique can increase the contrast more than the ASSVCR. Moreover, the tri-scan can also increase the overall intensity of the images.

### *6.3.3 Time complexity*

The time that is required to generate an enhanced color image for different image sizes using the proposed ASSVCR and tri-scan techniques are shown in Table 6.16. The experiment

was conducted on a PC having Intel (R) Pentium(R) dual CPU @ 2.00GHz and 6 GB of RAM. Here, it is noticeable that tri-scan is faster than ASSVCR. The average simulation time of tri-scan for 256×256 images is approximately 4 seconds and for 512×512 images, is approximately 16 seconds.

**Table 6.16 Comparison of simulation speed between two proposed techniques**

| Methodology | Image size | Step 1 | Step 2 | Total time (sec) |
|---|---|---|---|---|
| | | Enhancement time (sec.) | Color reproduction time (sec.) | |
| ASSVCR | 256x256 | 1.909 | 20.614 | 22.523 |
| | 512x256 | 2.597 | 40.119 | 42.716 |
| | 512x512 | 3.182 | 81.779 | 84.961 |
| Tri-scan | 256x256 | 4.17 | - | 4.17 |
| | 512x256 | 8.29 | - | 8.29 |
| | 512x512 | 15.87 | - | 15.87 |

In summary, in terms of the contrast level increment and sharpening, tri-scan is better, but can only be implemented on the color endoscopic images. Additionally, pseudo color is added in the images. Furthermore, the tri-scan is faster or has less time complexity compared to the ASSVCR technique. The ASSVCR cannot increase the contrast level and sharpening as much as tri-scan technique ; however, it is better for the situation where endoscopic images need to be enhanced with original color tone. Additionally, the ASSVCR technique can enhance and reproduce color in grayscale endoscopic images. Furthermore, it is very useful in saving power consumption during transmission in WCE.

# Chapter 7: Conclusion and future work

## 7.1 Conclusion

This chapter presents the summary of the project accomplishments. Two different color image enhancement techniques are developed to overcome the non-uniform brightness and poor color contrast problems, and to enhance the texture information of endoscopic images that highlight pit patterns, lesions, defected polyps, mucosa structures, tissue and vascular characterization.

At first, the endoscopic image enhancement based on adaptive sigmoid function and space-variant color reproduction (ASSVCR) is presented. It is achieved in two stages: image enhancement at gray level followed by space variant chrominance mapping based color reproduction. Image enhancement is done in two steps: adaptive sigmoid function and uniform distribution of sigmoid pixels. Then, space variant color reproduction is performed by generating a real color map by transferring and modifying old chrominance values, either from theme image or input image. In the second method, another color image enhancement technique named as tri-scan technology is presented for endoscopic images. It is achieved in three stages: (1) Tissue and surface enhancement, (2) Mucosa layer enhancement, (3) Color tone enhancement. At first, a modified linear unsharp masking is used to sharpen the surface and edges of tissue and vascular characteristics. Then, an adaptive sigmoid function is employed on the R plane of the image to highlight the subtle layers of the mucosa. Finally, the pixels are uniformly distributed to create a different color effect to highlight the subtle mucosa layers, mucosa structures and tissue characteristics which eventually assist gastroenterologists to identify some abnormalities and tissue characteristics accurately.

The ASSVCR technique enhances low contrast endoscopic images with original color tone, highlighting the pit patterns, abnormal growths, vascular and tissue characteristics of the endoscopic images. The infected areas surrounding the defected polyps and ulcers (as shown in Fig. 5.1 (1, 2 and 3)) are highlighted. Additionally, the ASSVCR enhances low contrast grayscale endoscopic images, in which color information is not available, and then reproduces color information from a theme image collected from the same or similar physical location of GI tract. Furthermore, it enhances and reproduces color on grayscale NBI images, thus, abnormal growths are more enhanced (as shown in Fig. 5.3). Moreover, the proposed color reproduction method is very useful in saving power consumption during the transmission in WCE. Instead of transmitting all color images from the WCE, the ASSVCR technique can only transmit one color image at the beginning, followed by a set of grayscale images. Later, in the computer, the grayscale images are colorized successfully using the first transmitted color image, as shown in Fig. 5.4.

The tri-scan technique enhances the color endoscopic images. It highlights the pit patterns, tissue and vascular characteristics, and distinguishes them with different pseudo colors. It also highlights micro-vessels of the superficial layers of the mucosa and sub-mucosa, creating a light steel blue effect in the background, an indian red effect on the mucosa structures and royal blue effect on the subtle mucosa layers. As a result, the mucosal surfaces and structures become more visible when compared to the original images. In NBI images, the superficial layers of the mucosal and pit patterns are seldom visible (as shown in Fig. 5.6 (1, 3 and 4)). In contrast, the tri-scan is capable of enhancing and highlighting the superficial layers of mucosal and pit patterns (as shown in Fig. 5.6 (1, 3 and 4)). Similarly, the FICE algorithm cannot always

highlight the mucosa surfaces and structures in the endoscopic images, but the tri-scan is able to consistently highlight the structures of mucosa surface (as shown in Fig. 5.7 (1 and 2)).

In summary, both techniques are suitable for enhancing and highlighting different features of endoscopic images; however, they have different methodologies. To enhance grayscale images or color endoscopic images with original color tones, the ASSVCR is more appropriate. Alternatively, the tri-scan technique is more applicable for enhancing color endoscopic images with pseudo colors.

## 7.2 Future work

This section provides a few recommendations which can be explored in future for improving in the performance of the color image enhancement techniques:

1. In this thesis, the performance of both techniques is evaluated using several objective performance metrics. However, the accuracy, specificity and sensitivity of the proposed techniques are not assessed, which left for future exploration.
2. The proposed color image enhancement techniques cannot preserve the brightness of the endoscopic images with over illumination exposure. In that case, different brightness preserving algorithms can be tested to preserve the brightness of those images that are over exposed during image acquisition.
3. The proposed techniques can assist in different computer aided detection (CAD) system to increase the amount of feature segmentation and classification of bleeding regions and abnormal growths.

# Appendix: List of publications

## A.1 Published peer reviewed conferences

*(* indicates related with this thesis)*

1. M. S. Imtiaz, and Khan A. Wahid, “A color reproduction method with image enhancement for endoscopic images,” *in Proc. IEEE 2nd Middle East Conf. on Bio-med. Engr.*, Feb. 2014. *

2. M. S. Imtiaz, T. H. Khan, and Khan A. Wahid, "New color image enhancement method for endoscopic images," *in Proc. IEEE Int. Conf. on Advances in Elect. Engr.*, pp. 263-266, 19-21 Dec. 2013. *

3. M. S. Imtiaz, and Khan A. Wahid, “Image Enhancement and Space-Variant Color Reproduction Method for Endoscopic images using Adaptive Sigmoid Function,” *in Proc. IEEE 36$^{th}$ Annual Engr.. In Med. and Bio. Society*, 26-30 Aug., 2014. *

4. M. S Imtiaz, R. Shrestha, et. al., "Cardiac cycle and heart rate calculation based on seismocardiogram," *in Proc. IEEE Canadian Conf. on Elect. and Compt. Engr.*, pp.1-5, May 2013.

5. M.S. Imtiaz, R. Shrestha, et. al., "Correlation between seismocardiogram and systolic blood pressure," *in Proc. IEEE Canadian Confr. on Elect. and Compt. Engr.*, pp.1-4, May 2013.

6. M. S. Imtiaz and B. Barua, “Transceiver circuits for pulse based ultra wideband,” *in Proc. Confr. on Engr. Resrh., Innov. and Edu.*, pp. 94-98, September, 2011.

# References


[1] A. Brownsey and J. Michalek, "High defination scopes, narrow band imaging, chromoendoscopy," *American Society of Gastrointestinal Endoscopy*, Nov. 2010.

[2] H. A. o. H. Kong, Ed., *Cancer statistics*. Hong Kong Registry, 2007.

[3] G. Pan and L. Wang, "Swallowable Wireless Capsule Endoscopy: Progress and Technical Challenges," *Gastroenterology research and practice* , pp. 1-9, Oct. 2011.

[4] R. M. Elena, et al., "Current status of device-assisted enteroscopy: Technical matters, indication, limits and complications," *World Journal of Gastrointestinal Endoscopy*, vol. 4, no. 10, pp. 453-461, Oct. 2012.

[5] D. G. Hewett and D. K. Rex, "Cap-fitted colonoscopy: a randomized, tandem colonoscopy study of adenoma miss rates," *Gastrointestinal Endoscopy*, vol. 72, pp. 775-781, 2010.

[6] A. Brownsey and J. Michalek, "Wireless capsule endoscopy," *American Society of Gastrointestinal Endoscopy*, Nov. 2010.

[7] B. Li and M. Q. H. Meng, "Wireless capsule endoscopy images enhancement via adaptive contrast diffusion," *Journal of Visual Communication and Imgae Representation*, vol. 23, no. 1, pp. 222-228, Jan. 2012.

[8] T. Kaltenbach, Y. Sano, S. Friedland, and R. Soetikno, "American Gastroenterological Association (AGA) Institute technology assessment on image-enhanced endoscopy," *Gastroenterology*, vol. 134, pp. 327-340, 2008.

[9] M. Meng, et al., "Wireless robotic capsule endoscopy: State-of-the-art and challenges," *Intelligent Control and Automation*, vol. 6, pp. 5561-555a, 2004.

[10] X. Xiang, G. Li, and Z. Wang, "Low-complexity and high-efficiency image compression algorithm for wireless endoscopy system," *Journal of Electronic Imaging*, vol. 15, pp. 023017-023017-15, 2006.

[11] D. Litwiller, "CMOS vs. CCD: maturing technologies, maturing markets," *Photonics Soectra*, vol. 39, no. 8, 2005.

[12] S. Lianpunsakul, V. Chadalawada, D. K. Rex, D. Maglinte, and J. Lappsa, "Wireless capsule endoscopy detects small bowel ulcers in patients with normal results from state of the art enteroclysis," *The American journal of gastroenterology*, vol. 98, pp. 1295-1298, 2003.

[13] P. Swain, "Wireless capsule endoscopy and crohn's diseases," *GUT*, vol. 54, pp. 323-326, Mar. 2005.

[14] S. Schmitz-valckenberg, F. G. Holz, A. C. Bird, and R. F. Spaide, "Fundus autofluorescence imaging: review and perspectives," *Retina*, vol. 28, no. 3, pp. 385-409, Mar. 2008.

[15] J. Pohl, A. May, T. Rabenstein, O. Pech, and C. Ell, "Computed virtual chromoendoscopy: a new tool for enhancing tissue surface structures," *Thieme E-Journals - Endoscopy*, vol. 39, no. 1, pp. 80-83, Jan. 2007.

[16] H. Chiu, et al., "A prospective comparative study of narrow-band imaging, chromoendoscopy, and conventional colonoscopy in the diagnosis of colorectal neoplasia," *GUT internatioanl Journal of gastroenterology and Hematology*, vol. 56, no. 3, p. 373, Sep. 2007.

[17] W. Curvers, et al., "Chromoendoscopy and Narrow-Band Imaging Compared With High-Resolution Magnification Endoscopy in Barrett's Esophagus," *Elsevier - Gastroenterology*,

vol. 134, no. 3, pp. 670-679, Mar. 2008.

[18] H. Machida, et al., "Narrow-band imaging in the diagnosis of colorectal mucosal lesions: a pilot study," *Endoscopy*, vol. 36, pp. 1094-1098, Dec. 2004.

[19] S. J. Chung, et al., "Comparison of detection and miss rates of narrow band imaging, flexible spectral imaging chromoendoscopy and white light at screening colonoscopy: a randomised controlled back-to-back study," *Gut* , vol. 63, pp. 785-791, May 2014.

[20] B. Li and M. Q. Meng, "Texture analysis for ulcer detection in capsule endoscopy images," *Image Vision Computing*, vol. 27, pp. 1336-1342, 2009.

[21] A. Allen and D. Snary, "The structure and function of gastric mucus," *Gut*, vol. 13, pp. 666-672, Aug. 1972.

[22] M. Igarashi. Advanced endoscopic imaging technologies. [Online]. http://www.naefrontiers.org/File.aspx?id=43577

[23] R. Ishihara, et al., "Autofluorescence imaging endoscopy for screening of esophageal squamous mucosal high-grade neoplasia: A phase II study," *Journal of Gastroenterology and Hepatology*, vol. 27, no. 1, pp. 86-90, Jan. 2012.

[24] H. Suzuki, et al., "Comparison of narrowband imaging with autofluorescence imaging for endoscopic visualization of superficial squamous cell carcinoma lesions of the esophagus," *Diagnostic and Therapeutic Endoscopy*, 2012.

[25] D. F. Boerwinkel, et al., "Effects of autofluorescence imaging on detection and treatment of early Neoplasia in patients With Barrett's Esophagus," *Clinical Gastroenterology and Hepatology*, vol. 12, pp. 774-781, 2014.

[26] T. Kouzu. (2007, Oct.) Fujinola, Atlas of spectral Endoscopic images (FICE). [Online].

http://www.fujinonla.com/inc/class/descargar.php?url=/archivos/catalogos/fice-atlas-esp.pdf

[27] S. J. Chung, et al., "Efficacy of computed virtual chromoendoscopy on colorectal cancer screening: a prospective, randomized, back-to-back trial of Fuji Intelligent Color Enhancement versus conventional colonoscopy to compare adenoma miss rates," *Gastrointestinal endoscopy*, vol. 72, no. 1, pp. 136-142, 2010.

[28] S. M. Pizer, et al., "Adaptive histogram equalization and its variations," *Computer Vision, Graphics, and Image Processing*, vol. 39, no. 3, pp. 355-368, 1987.

[29] K. Zuiderveld, "Contrast limited adaptive histogram equalization," *Graphics gems IV, Academic press professional, Inc.*, pp. 474-485, 1994.

[30] R. Srivastava, J. R. P. Gupta, H. Parthasarthy, and S. Srivastava, "PDF based unsharp masking, crispening and high boost filtering of digital images," *Communications in computer and information science*, vol. 40, pp. 8-13, 2009.

[31] D. Sheet, S. Garud, A. Suveer, M. Mahadevappa, and J. Chatterjee, "Brightness preserving dynamic fuzzy histogram equalization," *in proceeding of IEEE Transactions on Consumer Electronics*, vol. 56, no. 4, pp. 2475-2480, Nov. 2010.

[32] A. Carbonaro and P. Zingaretti, "A comprehensive approach to image contrast enhancement," *in proceeding of IEEE International Conference on Image Analysis and Processing*, pp. 241-246, 1999.

[33] H. Ibrahim and N. S. P. Kong, "Brightness Preserving Dynamic Histogram Equalization for Image Contrast Enhancement," *in proceeding of IEEE Transactions on Consumer Electronics*, vol. 53, no. 4, pp. 1752-1758, Nov. 2007.

[34] V. Magudeeswaran and C. G. Ravichandran, "Fuzzy Logic-Based Histogram Equalization

for Image Contrast Enhancement," *Mathematical Problems in Engineering*, p. 10, 2013.

[35] T. Welsh, M. Ashikhmin, and K. Mueller, "Transferring Color to Greyscale Images," *ACM Transactions on Graphics* , vol. 21, no. 3, pp. 277-280, Jul. 2002.

[36] T. Horiuchi and S. Hirano, "Colorization algorithm for grayscale image by propagating seed pixels," *in proceeding of the IEEE International Conference on Imgae Processing*, pp. 457-460, 2003.

[37] A. Levin, D. Lischinski, and Y. Weiss, "Colorization using optimization," *ACM Transactions on Graphics* , vol. 23, no. 1, pp. 689-694, 2004.

[38] V. korostyshevskiy. (2006) Grayscale to RGB converter. [Online]. www.mathworks.com/matlabcentral/fileexchange/13312-grayscale-to-rgb-converter

[39] M. S. Imtiaz and K. Wahid, "A color reproduction method with image enhancement for endoscopic images," *in proceeding of IEEE Conference on Biomedical Engineering*, pp. 135-138, Aug. 2014.

[40] M. S. Imtiaz, T. H. Khan, and K. Wahid, "New color image enhancement method for endoscopic images," *in proceeding of the IEEE International Conference on Advances in Electrical Enginering*, pp. 263-266, Dec. 2013.

[41] M. S. Imtiaz and K. Wahid, "Image enhancement and space-variant color reproduction method for endoscopic images using adaptive sigmoid function," *in proceeding of IEEE Engineering in Medicine and Biology Society*, Aug. 2014.

[42] A. Plaza, et al., "Recent advances in techniques for hyperspectral image processing," *Remote sensing of environment*, vol. 113, pp. 110-112, 2009.

[43] N. Hassan and N. Akamatsu, "A new approach for contrast enhancement using sigmoid

function," *International Arab Journal of Information Technology*, vol. 1, no. 2, pp. 221-225, Jul. 2014.

[44] P. Saruchi, "Adaptive Sigmoid Function to Enhance Low Contrast Images," *International Journal of Conputer Application*, vol. 55, no. 4, pp. 45-49, Oct. 2012.

[45] J. A. Yule, G. G. Field, and J. A. C. Yule, *Color: An Introduction to Practice and Principles*. John Wiley & Sons, 2012.

[46] B. A. Wandell and L. D. Silverstein, *The Science of Color*, D. O. S. A. 2nd ed. Washington, Ed. 2003.

[47] F. H. Imai and R. S. Berns, "Spectral estimation using trichromatic digital cameras," *in proceeding of International Symposium on Multispectral Imaging and Color Reproduction*, vol. 42, 1999.

[48] T. Luft, C. Colditz, and O. Deussen, "Image Enhancement by Unsharp Masking the Depth Buffer," *ACM Transactions on Graphics*, vol. 25, no. 3, pp. 1206-1213, 2006.

[49] Gastrolab – the gastrointestinal site. [Online]. http://www.gastrolab.net/index.htm.

[50] Atlas of Gastrointestinal Endoscopy. [Online]. http://www.endoatlas.com/index.html.

[51] X. Xu, Y. Wang, J. Tang, X. Zhang, and X. Liu, "Robust Automatic Focus Algorithm for Low Contrast Images Using a New Contrast Measure," *Sensors*, vol. 11, no. 9, pp. 8281-8294, Aug. 2011.

[52] C. H. Shen and H. H. Chen, "Robust focus measure for low-contrast images," *in proceeding of IEEE international Conference on Consumer Electronics*, pp. 69-70, 2006.

[53] B. Balas, L. Nakano, and R. Rosenholtz, "A summary-statistic representation in peripheral vision explains visual crowding," *Journal of Vision*, vol. 9, no. 12, pp. 1-18, Nov. 2009.

[54] C. D. Manning and H. Schutze, *Foundations of Statistical Natural Language Processing*, M. press, Ed. 1999.

[55] H. Ney, S. Martin, and F. Wessel, *Statistical language modeling using leaving-one-out*. Springer Netherlands, 1997.

[56] A. R. Robertson, "Historical development of CIE recommended color difference equation," *Color Research & Application*, vol. 15, no. 3, pp. 197-170, Jun. 1990.

[57] Z. Wang, A. C. Bovik, H. R. Sheikh, and E. P. Simoncelli, "Image quality assessment: from error visibility to structural similarity," *IEEE Transactions on Image Processing*, vol. 13, no. 4, pp. 600-612, 2004.

[58] Y. Shi, Y. Ding, R. Zhang, and J. Li, "Structure and hue similarity for color image quality assessment," *in proceeding of IEEE International Conference on Electronic Computer Technology*, pp. 329-333, 2009.

[59] S. E. Susstrunk and S. Winkler, "Color image quality on the internet," *In proceeding of International Society for Optics and Photonics*, pp. 118-131, Jan. 2003.

[60] T. Yada, C. Yokoi, and N. Uemura, "The Current State of Diagnosis and Treatment for Early Gastric Cancer," *Diagnostic and Therapeutic Endoscopy*, vol. 2013, p. 9, 2013.